CoA REPORT MAT. No. 3

THE COLLEGE OF AERONAUTICS

CRANFIELD

THE WELD HEAT AFFECTED ZONE STRUCTURE AND PROPERTIES OF TWO LOW CARBON Mn-Cr-Mo-V STEELS

by

E. Smith, L. J. Brown and R. L. Apps

CoA REPORT MAT No. 3
February, 1968.

THE COLLEGE OF AERONAUTICS
CRANFIELD

The Weld Heat Affected Zone Structure and Properties of Two Low Carbon Mn-Cr-Mo-V Steels

by

E. Smith, Ph.D., B.Sc., A.I.M.,
L.J. Brown, A.I.M.Mech.E., A.I.M.,
R.L. Apps, Ph.D., B.Sc., F.I.M., A.M.Inst.W.

SUMMARY

The visible weld heat affected zone (HAZ) of a low carbon, Mn-Cr-Mo-V steel was shown to be made up of four distinct regions; (a) the region of grain coarsening, (b) the region of grain refinement, (c) the region of partial transformation, and (d) the region of spheroidisation. Representative structures from the weld HAZ were reproduced, by means of a thermal simulation technique, in specimens large enough for mechanical testing. The thermal cycles applied were determined on a submerged arc bead-on-plate weld in $1\frac{1}{2}$" thick plate using a heat input of 108 kilojoules/inch.

Metallurgical examination and hardness measurements on two steels of this type showed that the simulated regions were comparable with the actual regions of the weld HAZ. The mechanical properties of the simulated HAZ regions were measured and correlated with the metallurgical microstructures.

In one of the steels embrittlement occurred in all regions of the HAZ, the region of grain coarsening being the most embrittled.

In the other steel a marked improvement in resistance to brittle fracture occurred in those regions which underwent a refinement of structure, but the region of grain coarsening suffered embrittlement. A subsequent heat treatment in the range 600°C - 645°C produced a severe embrittlement in all regions heated above the upper critical temperature and this was found to be a consequence of secondary hardening and a coarsening of the structure.

Regions of the weld heated to peak temperatures below the lower critical temperature were shown, using the simulation technique, to undergo a slight increase in strength and decrease in ductility but this was not serious.

Finally, an investigation was made of the secondary hardening behaviour of one of the steels having a high V content. A secondary hardness peak was observed on tempering between 600°C and 675°C.

CONTENTS

CONTENTS continued

1. Introduction

Low carbon, low alloy, Mn-Cr-Mo-V steels, marketed under the name of Ducol, were developed by Colvilles Ltd. to meet the demand for large high-tensile steel plates up to 6 inch. thick for use in pressure vessels and boiler drums operating at temperatures below the creep range. Existing steels failed to fulfill the necessary requirements of adequate strength at operating temperatures coupled with good weldability, ease of handling and bending, and low cost. The use of Ducol in pressure vessels instead of a C-Mn steel permits a reduction in plate thickness of up to 40%, and adequate weldability is ensured by limiting the carbon content to 0.17% maximum and imposing maximum limits on the alloy content.

Ducol is a basic open-hearth semi-air-hardening steel, i.e. its optimum properties are obtained by normalising and tempering. Its proof stress values at room and elevated temperature are markedly superior to those of a C-Mn steel which possesses the same tensile strength at room temperature. For example, boiler drums constructed from this material by John Thompson (Wolverhampton) Ltd. are designed to withstand a pressure of 2,780 p.s.i. at 365^{o}C and when fully fabricated they undergo a twelve hour leak hydraulic test at a pressure of 4,170 p.s.i. [1]

McKenzie [2] showed that butt welds in this material are normally satisfactory, but HAZ cracking was observed in fillet welds. This was attributed to the hardening associated with fast rates of cooling and its severity was dependent on the carbon content. Cracking in multi-run fillet welds of Ducol was also reported by Nicholls. [3]

McKenzie [2] also demonstrated that HAZ cracking was a serious risk in butt welds when rutile-coated electrodes were used, but this could be eliminated by either the use of preheat or the use of low-hydrogen electrodes. Normally a preheat to 200^{o}C and a post-weld heat treatment at about 650^{o}C are recommended for Ducol.

The work described in this report is part of a research programme being carried out at the College of Aeronautics, Cranfield, and sponsored by the Science Research Council, to investigate the relationship between microstructure and mechanical properties in the weld HAZ of low alloy steels. Ducol was considered a suitable choice for this programme because of its increasing industrial use and the lack of data on its weld HAZ properties. This was emphasized by the catastrophic failure of a pressure vessel at John Thompsons (Wolverhampton) Ltd., in December 1965 which formed the basis of a comprehensive B.W.R.A. report. [4]

The apparatus [5] developed at the College of Aeronautics, Cranfield, for subjecting specimens of a suitable size for mechanical testing to thermal cycles recorded in the actual HAZ of a weld in 1$\frac{1}{2}$" thick plate, was used. Notch-impact, tensile, and hardness properties of the various regions of the weld HAZ in two types of Ducol were measured and compared with the parent plate properties. An attempt was made to relate the changes in mechanical properties with microstructural changes.

Two factors were found to have a marked influence on transition temperature-hardness and grain size. In the regions of the weld HAZ experiencing peak temperatures below about 1100°C, where a considerable refinement of the structure was observed, these factors acted in opposition. The grain size effect was predominant, so that an overall decrease in transition temperature occurred. In the regions experiencing higher temperatures a coarsening of the microstructure was observed. This reinforced the embrittlement due to the hardened microstructure, so that the worst combination of mechanical properties was observed in these regions.

A small surplus of one of the steels permitted a few measurements to be made of the changes in tensile properties associated with thermal cycles having peak temperatures below the Ac_1. These are reported and discussed briefly. A small increase in strength and reduction in ductility were observed where the peak temperatures had exceeded about 300°C.

Finally the effect of a simulated post-weld heat treatment was investigated on one of the steels having a high vanadium content. This aspect of the work is still being pursued but already some important effects have been observed. This treatment has had a softening effect on the region of partial transformation leading to a reduction in the transition temperature. A softening was also observed in the grain refined region but this was accompanied by a marked coarsening of the structure, the overall effect being a considerable increase in the transition temperature. Secondary hardening was observed in regions of the weld HAZ experiencing peak temperatures above the Ac_3 and this, coupled with a coarsening of the structure, led to a considerable raising of the transition temperature.

2. Experimental

2.1 Materials

Two plates of Ducol from different casts were used in the present work. The first, which was designated Ducol W30, was supplied as a 3" thick plate. This will be referred to as 'Material A'. For the weld preparation this was milled down to 2" thickness to conform with the thickness of the mild steel plates on which the weld thermal cycles were measured. The initial condition of this material was unknown, but preliminary tensile tests and microscopical examination suggested that it was in the normalised condition, and so a tempering treatment of 2 hours at 650°C was carried out.

The second material, which was designated Ducol BW87A, was supplied as 2" thick plate and had been normalised at 950°C and tempered at 650°C for 3 hours, with a total tempering time aobve 600°C of 6 hours. This will be referred to as 'Material B'.

The chemical composition and mechanical properties of both materials in the 'as received' condition are shown in Tables I and II. Attention is drawn to the Vanadium content of Material B which was above the maximum allowed for in the specification. The specification for mechanical properties is given in Table II.

	C	Si	Mn	S	P	Ni	Cr	Mo	V
Material A (Ducol W30)	.14	.26	1.27	.027	.016	.25	.60	.28	n.d.
Material B (Ducol BW87A)	.14	.21	1.38	.021	.028	n.d.	.60	.29	.15
Maximum allowed in specification	.17	.30	1.50	.050	.050	.30	.70	.28	.10

TABLE I Chemical compositions of parent plate materials

		.2% Proof Stress	U.T.S.	Elongation	Reduction of Area
Material A (Ducol W30)	As received (normalised)	-	44.4 t.s.i.	28%	33%
	Tempered at 650°C	-	36.4 t.s.i.	35%	35%
Material B (Ducol BW 87A)	As supplied by manufacturer	28.8 t.s.i.	39.6 t.s.i.	31%	62%
	As tested in laboratory	30.6 t.s.i.	41.3 t.s.i.	-	68%
Specification	Transverse	22.5 t.s.i. at 120°C	36/42 t.s.i.	-	-

TABLE II Mechanical properties of parent plate materials

2.2 Experimental Procedure

The experimental procedure was similar to that described in detail in a previous report. [6] A summary only is given here.

2.2.1 Preparation and examination of weld

In order to examine the range of microstructures produced in the visible weld HAZ a bead-on-plate weld was made on Material A using a submerged arc welding unit and a heat input of 108 kilojoules per inch. A transverse section of the weld was prepared for metallographic examination using the conventional grinding and polishing techniques.

2.2.2 Mechanical properties of the weld HAZ

This was confined to hardness testing because of the minute size of the various regions of the HAZ. The hardness tests were carried out on a Zwick hardness tester using a load of 5 kilograms. Hardness determinations were made at 0.5 mm. intervals starting from the fusion boundary.

2.2.3 Simulation of weld HAZ structures

Structures representing four different parts of the visible weld HAZ were reproduced in un-notched Charpy-sized specimens of both materials using the simulation technique developed at Cranfield. [5] The peak temperatures associated with these structures were 788°C, 893°C, 1088°C and 1347°C. Details of the temperature measurement have been described by Coward and Apps. [7]

2.2.4 Metallographic examination of the simulated weld HAZ structures

An extensive metallographic examination, consisting of optical microscopy and electron microscopy of carbon replicas, was made on each of the simulated HAZ structures. These were compared with the structures observed in the actual weld HAZ.

2.2.5 Mechanical properties of the simulated weld HAZ structures

Charpy V-notch impact tests were carried out over a wide range of temperatures on specimens of each of the simulated weld HAZ structures. The variation of impact energy and fracture appearance with temperature was noted and transition temperatures calculated.

The mechanical properties were further investigated by means of hardness and tensile tests, the latter using the No. 13 Hounsfield test pieces with a shortened gauge length of 0.3" described in a previous report. [6]

2.2.6 Tensile properties of regions outside the visible weld HAZ

A few exploratory tensile tests were carried out on specimens of Material A simulated through thermal cycles measured outside the visible weld HAZ. The peak temperatures of these cycles varied from 200°C to 656°C.

The modified Hounsfield No. 13 test pieces were used.

2.2.7 The effect of a simulated post-weld heat treatment

Samples of Material B were given a simulated post-weld heat treatment by heating specimens simulating each of the 4 visible weld HAZ structures in an electric hump furnace. The temperature was raised to 645°C in 75 mins. and held between 600°C and 645°C for 100 mins. The cooling rate was 75°C per hour for the first hour. Temperature control was accurate to ±20°C. Charpy V-notch impact, tensile and hardness tests and metallographic examination were then carried out to study the effect of this treatment.

2.2.8 Secondary hardening in the grain coarsened region

The marked increase in hardness and transition temperature in the grain coarsened region resulting from the simulated post-weld heat treatment, and the comparatively high Mo and V contents of the parent material, suggested that secondary hardening was occurring at the temperatures normally used for post-weld heat treatment.

To examine this more closely, ageing curves were determined on material simulating the grain coarsened region at temperatures of 500°C, 600°C, 650°C, 675°C and 700°C. The variation of hardness with time at these temperatures was recorded. These tests were carried out on the broken Charpy specimens due to shortage of material. This also limited the extent of this part of the programme to hardness testing.

3. Results

3.1 Metallography and Hardness of the Weld HAZ

The parent plate microstructures of both materials were typical of hot rolled structures and consisted of banded ferrite and carbide. At high magnifications the carbide areas resolved into a bainite structure. These structures are shown in Figs. 1 and 7 for Material A and in Fig. 12 for Material B. These micrographs show that Material B had a coarser grain size than Material A.

The range of microstructures produced in Material A by the bead-on-plate weld is shown in Fig. 1. The HAZ could be divided into four distinct regions and these were identified in terms of their distance from the weld fusion boundary as follows:-

(a) The region of grain coarsening

This region extended from 0 to 1.1 mm. from the fusion boundary and experienced maximum temperatures in excess of 1100°C. Since the maximum temperatures were well into the austenite region, austenite grain growth had taken place, the effect being more marked with decreasing distance from the fusion boundary. The relatively rapid cooling rates experienced in these

regions were evidenced by the coarse Widmanstätten structures produced, as shown in Fig. 1(a).

(b) The region of grain refinement

This region extended from 1.1 to 2.0 mm. from the fusion boundary and experienced maximum temperatures in the approximate range of 1100°C to 900°C. Complete austenitization had occurred and a very fine structure of ferrite and carbide was produced. This is shown in Fig. 1(b).

(c) The region of partial transformation

This region extended from 2.0 to 3.6 mm. from the fusion boundary and experienced maximum temperature in the approximate range of 900°C to 750°C, the temperature limits of Ac_3 and Ac_1. Partial austenitization had occurred as the bainite areas were taken into solution. At the upper end of this temperature range much of the ferrite had also dissolved, producing a mixture of fine grained ferrite and carbide with some untransformed ferrite. At the lower end of this temperature range only the bainite areas had been visibly affected, the original ferrite remaining unchanged. This structure is shown in Fig. 1(c).

(d) The region of spheroidisation

At the extreme edge of the HAZ away from the fusion line a narrow region was observed in which spheroidisation of the bainite had occurred. The peak temperatures reached in this region were close to the effective Ac_1 point.

Beyond this region structural changes were not observed by optical microscopy and, therefore, limited the region defined as the weld HAZ.

The changes in hardness through the weld HAZ of Material A with increasing distance from the fusion boundary are shown in Fig. 2. This shows that the material was considerably hardened in the HAZ and, in general, the hardness increased with decreasing distance from the fusion boundary. Maximum hardness was located in the grain coarsened region.

3.2 Metallography of the Simulated Weld HAZ Structures

3.2.1 Material A

(a) Simulated to a peak temperature of 788°C

The structure produced by this treatment is shown in Fig. 3. This appears to be equivalent to the lower temperature part of the partially transformed region. The bainite areas were more diffuse than in the parent material due to partial dissolution and reprecipitation as a fine dispersion, as can be seen in the electron micrographs. The peak temperature experienced is likely to have been just above the effective Ac_1.

(b) Simulated to a peak temperature of 893°C

The structure produced by this treatment is shown in Fig. 4. A very fine structure of ferrite and carbide was produced and it seems likely that peak temperatures were just above the effective Ac_3. This appears to be equivalent to the region of grain refinement.

(c) Simulated to a peak temperature of 1088°C

The structure produced by this treatment is shown in Fig. 5. A fine acicular structure was formed, but this was much coarser than in the specimen cycled to 893°C. The prior austenite grain boundaries were clearly outlined suggesting that this is the start of the region of grain coarsening.

(d) Simulated to a peak temperature of 1347°C

The structure produced by this treatment is shown in Fig. 6. An acicular structure, much coarser than in the specimen cycled to 1088°C, was produced, suggesting that this represents a region close to the fusion boundary.

3.2.2 Material B

(a) Simulated to a peak temperature of 788°C

The structure produced by this treatment is shown in Fig. 8. An apparent tendency towards spheroidisation can be seen at all magnifications, suggesting that the peak temperature was very close to the effective Ac_1.

(b) Simulated to a peak temperature of 893°C

The structure produced by this treatment is shown in Fig. 9. A marked refinement of the structure had occurred and at high magnifications ferrite grains and strings of carbide were observed. This appears to represent the grain refined region with a peak temperature close to the effective Ac_3.

(c) Simulated to a peak temperature of 1088°C

The structure produced by this treatment is shown in Fig. 10. A fine structure was produced. At high magnifications this was seen to be acicular and the prior austenite grain boundaries were clearly visible. This appears to be the start of the grain coarsened region and peak temperatures were obviously above the Ac_3.

(d) Simulated to a peak temperature of 1347°C

The structure produced by this treatment is shown in Fig. 11. A coarse structure of ferrite and carbides of Widmanstätten appearance was produced indicative of peak temperatures associated with the region of grain coarsening.

3.3 Mechanical Properties of the Simulated Weld HAZ Structures

The hardness of the specimens of both materials simulated through the four thermal cycles are recorded with the micrographs, Figs. 3-12. The results of the Charpy V-notch impact tests are shown in Figs. 13-16 and the tensile tests in Figs. 17 and 18. The complete mechanical testing data are summarised in Tables III and IV.

3.4 Tensile Properties of Regions Outside the Visible Weld HAZ

The results of the tensile tests on specimens of Material A simulated through weld thermal cycles having peak temperatures between 200°C and 656°C are summarised in Table V.

3.5 The Effect of Post-Weld Heat Treatment on Material B

The effects of a post-weld heat treatment, in which specimens of Material B were heated between 600°C and 645°C for 100 minutes, after simulation to 788°C, 893°C, 1088°C and 1347°C, are shown in Figs. 19-28. Figs. 19-22 compare the Charpy V-notch impact properties before and after post weld-heat treatment for each region separately; tensile test results are shown in Fig. 23 and Figs. 24-38 show the microstructures observed.

3.6 Secondary Hardening in the Grain Coarsened Region of Material B

The changes in hardness with ageing time at temperatures between 500°C and 700°C for specimens of Material B simulating the grain coarsened region are shown in Fig. 29.

4. Discussion

Before attempting an assessment of the relationship between metallurgical structure and mechanical properties an attempt will be made to explain the microstructural changes. Two temperatures are specially relevant to the present discussion. These are the Ac_1 and the Ac_3 temperatures at which transformation to austenite begins and ends. These temperature limits serve as a useful guide to a classification of the transformations occurring in the weld HAZ of low alloy steels.

Andrews [8] has derived the following formulae for calculating the equilibrium values of the Ac_1 and Ac_3 temperatures for steels of varying composition:-

$$Ac_1 = 723 - 10.7\,Mn - 16.9\,Ni + 29.1\,Si + 16.9\,Cr + 290\,As + 6.38\,W$$

$$Ac_3 = 910 - 203\sqrt{C} - 15.2\,Ni + 44.7\,Si + 104\,V + 31.5\,Mo + 13.1\,W - 30\,Mn - 11\,Cr - 20\,Cu + 700\,P + 400\,Al + 120\,As + 400\,Ti$$

Treatment	0.2% Proof Stress (t.s.i.)	U.T.S. (t.s.i.)	Reduction of Area (%)	Elongation (%)	U.T.S./ Proof Stress	Hardness HV 10	Transition Temperature (^{o}C)	
							50% Xaly	20 ft.lbs.
As received	27.9	39.7	73	52.3	1.42	196	-15	-50
Cycled to 788^{o}C	37.5	51.4	60	49.3	1.37	214	19	-34
Cycled to 893^{o}C	-	-	-	-	-	341	15	-34
Cycled to 1088^{o}C	48.6	55.3	69	45.3	1.14	310	12	-39
Cycled to 1347^{o}C	51.4	58.6	68	45.7	1.14	298	56	- 1

TABLE III Mechanical properties of Material A simulated specimens

Treatment	0.2% Proof Stress (t.s.i.)	U.T.S. (t.s.i.)	Reduction of Area (%)	Elongation (%)	U.T.S./ Proof Stress	Hardness HV 10	Transition Temperature (^{o}C)	
							50% Xaly	20 ft.lbs.
As received	30.6	41.3	68	50.6	1.35	200	47	-16
Cycled to 788^{o}C	31.0	45.7	55	50.8	1.47	234	47	-15
Cycled to 893^{o}C	34.4	53.3	60	46.0	1.55	276	- 9	-82
Cycled to 1088^{o}C	40.3	55.9	61	45.6	1.39	288	20	-34
Cycled to 1347^{o}C	47.3	54.7	65	48.8	1.16	281	56	-10

TABLE IV Mechanical properties of Material B simulated specimens

Treatment	0.2% Proof Stress (t.s.i.)	U.T.S. (t.s.i.)	Reduction of Area (%)	Elongation (%)	U.T.S./ Proof Stress
As received	26.6	37.6	72	53.7	1.41
Cycled to 200°C	27.0	38.1	73	50.3	1.41
Cycled to 260°C	26.5	37.5	70	46.7	1.42
Cycled to 331°C	29.1	39.7	68	45.3	1.36
Cycled to 400°C	28.9	39.1	70	45.7	1.35
Cycled to 480°C	28.9	39.0	74	48.7	1.35
Cycled to 656°C	29.0	39.1	69	45.0	1.35

TABLE V Mechanical properties of Material A specimens simulated below the Ac_1 temperature

In these formulae the compositions are expressed as weight percentages.

Applying the formulae to the steels used in this work the following values are obtained:-

	Ac_1	Ac_3
Material A	723°C	817°C
Material B	724°C	840°C

Previous work [6] has shown that due to the rapid heating rates of about 200°C per second associated with the welding conditions used here, the Ac_1 and Ac_3 temperatures are raised by approximately 35°C and 75°C respectively. [3] This would suggest the following approximate values for the effective Ac_1 and Ac_3 temperatures for the Ducol materials:-

	Ac_1	Ac_3
Material A	758°C	892°C
Material B	759°C	915°C

Albutt and Garber [9] have pointed out that the shape and distribution of the carbides may influence the degree to which the Ac_3 is varied during rapid heating, but that the Ac_1 is insensitive to this. Several other factors, such as initial inhomogeneity and grain size may also affect the values of the Ac_1 and Ac_3 temperatures. However, with these limitations in mind, the above values of the effective Ac_1 and Ac_3 temperatures are now used to establish the relationship between the weld thermal cycles and the microstructural changes.

4.1 Metallography of the Weld HAZ

In those parts of the weld HAZ experiencing peak temperatures between the effective Ac_1 and Ac_3, i.e. for Ducol between about 760°C and 900°C, partial austenitization occurred to a greater or lesser extent. The lower temperature end of this region was bounded by the region of spheroidisation in which, as its name implies, spheroidisation of the carbides had occurred. This can be seen in Fig. 1. This region was associated with peak temperatures close to the Ac_1, i.e. $\sim$ 760°C in this case, and it is thought that either the carbides had begun to dissolve and precipitated as spherical particles on cooling, or that dissolution had started at the corner of the carbide grains thus producing a rounding effect in the final microstructure.

As the peak temperature was increased more and more carbide was transformed to austenite. Dilution of this high carbon austenite by the surrounding ferrite occurred as the equilibrium concentration of carbon in austenite gradually decreased with increasing temperature. As the temperature

approached the effective Ac_3 the ferrite became increasingly affected until, at the boundary of the region, all the structure had transformed.

This region, heated between the effective Ac_1 and Ac_3, was characterised on cooling by transformation occurring from a partially austenitized structure. At the lower temperature end of the region, the austenite contained up to about 0.8% carbon, thus transformation to martensite and/or bainite was expected. The presence of bainite in this region can be seen in Fig. 1(c).

Above the effective Ac_3 temperature a completely austenitic structure was produced. Homogenisation of the carbon then proceeded, but, due to the short duration of the thermal cycles, transformation from an inhomogeneous austenite occurred producing a fine grained structure as shown in Fig. 1(b). As the peak temperature continued to rise, austenitic grain growth occurred and the resulting structures became increasingly coarse as the fusion boundary was approached.

On subsequent fairly rapid cooling, proeutectoid ferrite was precipitated as large plates at the austenite grain boundaries. The austenite subsequently transformed to an acicular structure resembling upper bainite. The prior austenite grains were clearly outlined by the proeutectoid ferrite, as shown in Fig. 1(a).

4.2 Mechanical Properties of the Actual Weld HAZ Structures

The hardness survey across the actual weld HAZ of Material A, shown in Fig. 2, showed a considerable increase in hardness over that of the parent plate. The marked increase first became apparent when most of the ferrite had been austenitised during the heating cycle. In the grain refined region the hardened structure was associated with a fine mixture of ferrite and carbide. A maximum hardness of 360-370 HV 5 occurred near the fusion boundary and was associated with a coarse Widmanstätten distribution of ferrite and upper bainite.

4.3 Mechanical Properties and Microstructures in Material A Simulated Weld HAZ Regions

A comparison of the Charpy V-notch impact properties of the four simulated HAZ regions is shown in Figs. 30 and 31 and the changes in their 20 ft.lbs. and 50% crystallinity transition temperatures are shown in Fig. 32. The tensile properties are shown in Fig. 17 and Table III gives a complete summary of the mechanical testing data. The effect of thermal simulation to peak temperatures of 788°C, 893°C, 1088°C and 1347°C was to reduce the notch toughness and ductility, and to increase the proof stress, U.T.S., hardness, and transition temperature. In most cases these changes in mechanical properties were greater with increasing peak temperature of simulation.

The greatest value of hardness (341 HV-10) was associated with the peak temperature of 893°C. The hardness then fell to a value of 298 HV 10

for the region cycled to 1347°C. These results were at variance with those measured in the actual weld HAZ, although both showed a considerable increase over that of the parent plate. One possible significant difference between the hardness measurements in the actual weld and those on the simulated specimens, was that in the former the hardness impression was likely to embrace a range of structures, due to the steep temperature gradient prevailing during welding, while in the latter the hardness of a uniform structure was measured.

Explanations for the changes in mechanical properties are now given in terms of the observed microstructures.

(a) Thermal simulation to a peak temperature of 788°C

The peak temperature reached in this cycle, which just exceeded the Ac_1 point under these conditions of rapid heating, had effectively limited austenitization to the bainitic areas, with the ferrite grains remaining essentially unchanged. Since the time at which the specimen was above the Ac_1 temperature was very short (approximately 8 seconds) an inhomogeneous mixture of partially transformed bainite surrounded by high carbon austenite in a matrix of untransformed ferrite was produced.

During the short time above the Ac_1 temperature there was a tendency for the carbon-rich austenitic areas to grow at the expense of the surrounding ferrite due to the decreasing equilibrium concentration of carbon in austenite with increasing temperature above the Ac_1. On subsequent fairly rapid cooling the austenite, still rich in carbon transformed to a hardened structure, which in the extreme case would be expected to be martensitic. However the cooling rate associated with this particular thermal cycle was insufficient for martensite formation, and a fine bainitic structure was formed. The final microstructure shown in Fig. 3 consisted, therefore, of partially transformed bainite, newly produced bainite and ferrite, and untransformed ferrite. There was a slight increase in the bainitic areas at the expense of the ferrite. This had only a minor effect on the macrohardness of the structure, which was not surprising, since there were still large areas of ferrite that had been unaffected by the thermal cycle. These structural changes are more likely to have a significant effect on the other mechanical properties. This was reflected by the increases in transition temperature, proof stress and U.T.S., and the reduction in ductility compared to the parent plate material, as can be seen in the results summarised in Table III.

(b) Thermal simulation to a peak temperature of 893°C

On heating to this peak temperature austenitisation occurred to a much greater extent than in the previous thermal cycle, so that all the ferrite was transformed. The peak temperature was thus apparently just above the effective Ac_3, but insufficient time was available for complete homogenisation of the austenite to take place, as is evident from the low magnification photograph of the final structure shown in Fig. 4. On subsequent fairly rapid cooling the austenite transformed to a very fine mixture of ferrite and carbide

(Fig. 4). This brought about a large increase in hardness which was probably due to the large decrease in the size of the ferrite areas and the presence of transformation products of high carbon austenite.

On the basis of the grain size effect formulated by Petch [10, 11], this structure would be expected to give an appreciable reduction in transition temperature over that of the material cycled to 788°C. Table III, however, shows only an insignificant reduction. This may have been due to the presence still of some high carbon transformation products, which would have tended to raise the transition temperature. A closer look at the full transition curves (Figs. 30 and 31), however, shows that on the ductile side of the transition point, the notch-toughness properties have been considerably improved. This may be due to the increased energy required for the propagation of a fracture in a fine grained structure. Unfortunately no tensile properties were recorded for this thermal cycle.

(c) Thermal simulation to a peak temperature of 1088°C

On heating the parent material to this peak temperature, which was considerably in excess of the Ac_3, a fully austenitic structure was produced. Homogenisation had commenced, but because of the short time at which the temperature was above the Ac_3 (about 5 secs) this was not completed. On subsequent rapid cooling through the initial temperature range, a network of proeutectoid ferrite formed at the austenite grain boundaries and within this network a fine acicular structure resembling upper bainite appeared (Fig. 5). The resulting structure had a typical Widmanstätten appearance, although this was very fine because of the absence of marked grain growth during the austenitisation part of the thermal cycle.

The fracture toughness properties of this material were distinctly inferior to those of the parent material, but similar to those of the material cycled to 893°C. The similarity with the material cycled to 893°C was not surprising since they were both very fine structures of ferrite and carbide, although rather different in morphology. The lower hardness value compared to the material cycled to 893°C may have been due to the homogenisation of the austenite, leading to a more uniform distribution of the carbon. There was a considerable increase in strength and reduction in ductility compared to the parent plate, which would be expected from the Widmanstätten form of the structure and the high hardness associated with it.

(d) Thermal simulation to a peak temperature of 1347°C

Peak temperatures in this region greatly exceeded the Ac_3, so that homogenisation of the austenite was complete or near-complete, and marked grain growth took place. The subsequent rapid cooling rate produced a very coarse Widmanstätten structure, as shown in Fig. 6, consisting of a network of ferrite grains outlining the prior austenite grains and surrounding large areas of upper bainite. The tensile properties were not markedly different from those of the previous sample, but the notch-toughness properties were considerably worse. In fact the transition temperatures were about 50 - 70°C

higher than for the parent material. This was attributed to the coarse Widmanstätten character of the structure.

4.4 Mechanical Properties and Microstructures in Material B Simulated Weld HAZ Regions

A comparison of the Charpy V-notch impact properties of the four simulated HAZ regions is shown in Figs. 33 and 34 and the changes in their 20 ft.lbs. and 50% crystallinity transition temperatures in Fig. 35. The tensile properties are shown in Fig. 18 and a complete summary of the mechanical testing data in Table IV.

Of the four thermal cycles investigated those with peak temperatures of 788°C and 1347°C were observed to produce the highest transition temperatures, as was the case with Material A. However, a considerable decrease in transition temperature from that of the parent plate was observed in the material cycled to 893°C, and to a lesser extent that cycled to 1088°C. This effect was not observed in Material A.

A comparison of the parent plate properties of both materials suggests a possible explanation. Fig. 36 taken from a paper by McKenzie [2] shows the range of V-notch Charpy temperature/impact curves for a number of 5 inch. thick plates of Ducol. The curves for the Material A and Material B are also shown. The curve for Material A lies just outside the lower temperature boundary of the range quoted by McKenzie for 5 inch.-plate, while Material B lies at the other boundary of the range. The difference in their 20 ft.lbs. transition temperatures was approximately 40°C. The tensile properties, shown in Tables III and IV, indicated a slightly higher strength and lower ductility for Material B. These differences in parent plate properties may have been due to slight differences in the temperatures employed for normalising and tempering during manufacture. The B.W.R.A. investigation of the pressure vessel failure at John Thompsons (Wolverhampton) Ltd. demonstrated the criticality of these temperatures [4]. In terms of chemical composition, the most significant factor was probably the 0.15% of vanadium in Material B which was 50% above the maximum allowed for in the specification and could have contributed to this difference in mechanical properties. In addition the slightly coarser grain size of Material B would favour a higher transition temperature.

Explanations for the changes in mechanical properties occurring in the simulated weld HAZ have already been attempted for Material A. A few differences were observed with Material B and so the following comments supplement those already made for Material A.

(a) Thermal simulation to a peak temperature of 788°C

Fig. 8 indicates that the carbides had begun to dissolve producing a spheroidised structure. The estimate of the effective Ac_1 temperature under these conditions of rapid heating suggested that the peak temperature was just above the Ac_1. A slight increase in hardness and strength over that of the parent plate occurred, similar to Material A. In contrast to Material A,

however, no significant change in transition temperature from that of the parent plate was observed. This was probably due to the high transition temperature of the parent plate discussed above.

(b) Thermal simulation to a peak temperature of 893°C

Fig. 9 shows that this treatment produced a very fine homogeneous structure of ferrite and bainite, similar to the corresponding region in Material A. The transition temperature was reduced drastically compared to Material A, even after allowing for the high initial transition temperature of the parent plate. A comparison of the hardnesses of the two materials showed that Material B had a value of 276 HV 10 compared with a value of 341 for Material A. This agreed well with the values of transition temperature. A possible explanation for this softer structure in Material B may lie in the values of the effective Ac_3 temperatures. The calculations made earlier in the report indicated that the Ac_3 temperature for Material B was some 40°C above that for Material A. Thus, it may be that in the former material some untransformed ferrite still existed, which could have contributed to a softening effect on the structure. There appears to be some evidence of untransformed ferrite in the original ferrite bands in Fig. 9.

(c) Thermal simulation to a peak temperature of 1088°C

This structure, shown in Fig. 10, was similar to the corresponding one in Material A, except that it appeared to be rather fine, and the bainite had a more jagged appearance. The hardness value was significantly lower than in Material A and this was reflected in its lower transition temperature.

(d) Thermal simulation to a peak temperature of 1347°C

The structure, shown in Fig. 11 was very similar to the corresponding one in Material A, and the mechanical properties were also similar. Considering Material B alone, this thermal cycle produced the worst combination of mechanical properties, with a transition temperature some 10°C higher than the parent plate material, which itself had a high transition temperature.

4.5 Tensile Properties of Regions Outside the Visible Weld HAZ

Table V shows that thermal simulation to peak temperatures between 200°C and 656°C in Material A produced no marked change in tensile properties. At 200°C and 260°C there was a slight drop in elongation, but the proof stress and U.T.S. values were essentially unchanged. Above 260°C the proof stress increased by about 2.5 t.s.i. and the U.T.S. by about 1.5 t.s.i. with a further very slight drop in elongation. These results indicate that no serious embrittlement occurs outside the visible weld HAZ due to purely thermal effects, i.e. in the absence of strain and notch effects. However, this observation is not particularly relevant to welding conditions where the material is subjected to constraint imposed by the surrounding material. It is now generally accepted that it is a combination of heat and strain that causes embrittlement in the parent material outside the visible weld HAZ. This effect would be accentuated by the presence of stress-raisers.

4.6 The Effect of Simulated Post-Weld Heat Treatment on Material B

An actual specification for the stress relief of welds in Ducol used in the construction of a pressure vessel states [4]:-

"The sections will be placed in the furnace at a temperature not exceeding 300°C. It will then be heated at a rate not exceeding 50°C/hour to a stress-relieving temperature of 620/660°C where it will be soaked for a period of 1 hour/inch of shell thickness. The cooling rate to 300°C not to exceed 60°C/hour after which it can be cooled in still air."

The simulated post-weld heat treatment applied here and described in the experimental section differed slightly from the above procedure. The heating rate (up to 645°C in 75 minutes) was considerably faster, and the cooling rate (75°C/hour) was also slightly faster. But it seems probable that in these small scale tests it would be the peak temperature of the treatment which would be most effective. In this respect, the temperature range used here, 600°C - 645°C, was some 20°C lower than the recommended range.

The results of the mechanical tests are shown in Figs. 19 - 23. Table VI summarises the results before and after post-weld heat treatment. The treatment had different effects on the parent material and the four simulated regions, and so for convenience, each of these will be discussed separately.

(a) Parent plate

Simulated post-weld heat treatment made no apparent difference to the microstructure within the range of magnifications used (compare Figs. 12 and 24). Irvine and Pickering [12] have pointed out that low carbon bainitic steels show little change in microstructure when heated to temperatures below 650°C, but temperatures as high as 700°C can cause an increase in grain size accompanied by a marked decrease in hardness. There was a slight decrease in strength and increase in ductility accompanying the post-weld heat treatment. This was probably due to a further tempering effect on the initially normalised and tempered structures. Unfortunately there was insufficient material to produce comparable Charpy V-notch impact/temperature curves.

(b) Material thermally cycled to 788°C

A comparison of Figs. 8, 12 and 25 shows that after post-weld heat treatment the structure resembled that of the parent plate. This could occur if the weld simulation cycle produced supersaturation of some carbides by the rapid cooling rate after dissolution. These carbides could easily have reformed at temperatures in the range 600°C - 645°C. The similarity in the mechanical properties between these two structures supports this assertion.

A comparison of the mechanical properties of the material simulated to a peak temperature of 788°C, before and after post-weld heat treatment, shows that the post-weld heat treatment reduced the Charpy 20 ft.lbs. transition temperature by about 23°C, with a corresponding reduction in proof stress, U.T.S., and hardness, and increase in ductility. In describing the structures formed in the partially transformed region of the weld HAZ, it was shown that

	0.2% Proof stress (t.s.i.)	U.T.S. (t.s.i.)	Reduction of area (%)	Elongation (%)	Charpy 20 ft.lbs. temp.	Hd HV 10
As received	30.6	41.3	68	50.6	-16	200
As received + post heat	29.0	39.0	70	51.7	N.D.	198
788°C peak	31.0	45.7	55	50.8	-15	234
788°C peak + post heat	28.7	40.6	66	54.8	-38	200
893°C peak	34.4	53.3	60	46.0	-82	276
893°C peak + post heat	41.0	48.2	67	51.9	-46	261
1088°C peak	40.3	55.9	61	45.6	-34	288
1088°C peak + post heat	48.0	54.0	65	49.8	+24	300
1347°C peak	47.3	54.7	65	48.8	-10	281
1347°C peak + post heat	51.6	56.5	60	48.5	+51	295

TABLE VI Mechanical properties of Material B simulated weld heat affected zones before and after post weld heat treatment

the transformation products of a high carbon austenite could be expected in this region. The beneficial effect of the post-weld heat treatment was thus probably a reflection of the tempering effect on these transformation products.

(c) Material thermally cycled to 893°C

A comparison of Figs. 9 and 26 reveals a marked coarsening of the structure after post-weld heat treatment. The smaller transformed ferrite grains produced by the HAZ thermal cycle probably had orientations not very different from the larger primary ferrite grains from which they were formed. The subsequent post-weld heat treatment allowed the primary ferrite grains to grow at the expense of the smaller transformed ones, and carbides became clearly visible. These carbides were concentrated in small bainitic areas and along the ferrite grain boundaries. The size of many of the carbides

was as great as that of the carbides in the parent material. Fig. 26 shows them clearly at a magnification of 28,000, while at a magnification of 6,000 they can be seen to be much more dispersed than in the parent plate. Most of these carbides were either in solution or in small areas in a finely divided state after the simulated weld thermal cycle. Post-weld heat treatment allowed them to coalesce particularly at grain boundaries.

The reduction in hardness and U.T.S., and the increase in ductility after the post-weld heat treatment was indicative of the softening which had occurred. This was probably due to a tempering effect on those regions produced from a high carbon austenite during the weld thermal cycle. However, the marked coarsening of the structure after post-weld heat treatment appears to have had an over-riding effect on the transition temperature, which was increased by about 36°C.

(d) Material thermally cycled to 1088°C

A comparison of Figs. 10 and 27 reveals a slight coarsening of the structure. It may well be that the carbides had begun to coalesce, although extraction replicas of the material before post-weld heat treatment are not available for comparison.

The mechanical testing data appear to be rather contradictory and suggest that in using a tensile test piece with a shortened gauge length of 0.3" the restraint of the shoulders affected the stress/strain relationship at high strains. Thus, principal reliance was placed on the value of proof stress in the present case. This value increased considerably after the post-weld heat treatment, and was accompanied by an increase in hardness, and a large increase in transition temperature of 58°C. Two reasons are suggested for this. First an increase in the coarseness of the structure, which would probably be most effective in increasing the transition temperature, and secondly a secondary hardening effect caused by a combination of the high contents of Mo and V, and a rapid cooling rate from the austenitising temperature during the weld thermal cycle. It was established earlier in the report, that the grain coarsened region of the weld HAZ in this material was subjected to secondary hardening in the temperature range of approximately 600°C - 700°C. Such a phenomenon of secondary hardening could account for the changes observed in the mechanical properties.

(e) Material thermally cycled to 1347°C

Post-weld heat treatment appears to have had a similar effect to that described for the material thermally cycled to 1088°C. Because of its very coarse structure and high transition temperature after welding, post-weld heat treatment produced material with the poorest notch-impact properties.

4.7 Secondary Hardening in the Grain Coarsened Region of Material B

The results of the secondary hardness tests on material simulating the grain coarsened region showed that substantial hardening can occur at the normally recommended temperatures for post-weld heat treatment (cf. Fig. 29). This may have been due primarily to the high V content of .15%, which was

50% above the maximum allowed for in the specification.

Since the hardest and most brittle region of this material after welding was the grain coarsened region, any post-weld heat treatment should be aimed at improving the properties of this region in addition to the normal stress-relieving role. The secondary age-hardening curves indicated that at 650°C, 5 - 10 hours would be required to reduce the hardness below that of the material after welding. To produce a similar effect in a shorter time, then a temperature in the range 675°C - 700°C would be required. The presence of a hardened microstructure in the weld HAZ is a condition for the occurrence of HAZ cracks. Experience suggests that such HAZ cracks are only likely to form when the hardness of the microstructure is above 350 V.P.N., which is some 50 points higher than the maximum hardness found in Material B in the present investigation. However, it should be borne in mind that the welding conditions simulated in this work was for a high level of heat input (108 kilojoules per inch) and consequently these results do not preclude the possibility of the formation of a microstructure with a hardness value greater than 350 V.P.N. when using lower levels of heat input.

4.8 Further Work on Post-Weld Heat Treatment of Material B

A similar set of hardness-time curves to those shown in Fig. 36 are being determined for the parent plate and for material from the simulated weld HAZ experiencing peak temperatures of 788°C, 893°C and 1088°C. It is hoped that these results will help to clarify the reasons for the changes in mechanical properties observed with a simulated post-weld heat treatment in the present investigation.

5. Conclusions

1. The weld HAZ of both Ducol materials was divided into 4 distinct regions. These were (a) the region of grain coarsening, (b) the region of grain refinement, (c) the region of partial transformation, and (d) the region of spheroidisation.

2. In the visible weld HAZ of Material A, the hardness values were increased considerably above that of the parent plate. Values in the range 300 - 370 H.V.5, occurred from the grain refined region to the fusion boundary.

3. Microstructures and hardness measurements showed that the simulated weld HAZ compared favourably with the actual weld HAZ in Material A.

4. Material A simulated to peak temperatures of 788°C, 893°C, 1088°C and 1347°C had inferior Charpy V-notch toughness compared with the parent plate. This was attributed, at the lower temperatures, to the formation of bainite from high carbon austenite and at the higher temperatures to the formation of a coarse Widmanstätten structure of proeutectoid ferrite and upper bainite.

5. In Material A the proof stress and U.T.S. increased and the ductility decreased as the peak temperature of simulation increased. Thus the worst

combination of mechanical properties occurred in the grain coarsened region heated to temperatures close to the melting point.

6. Material B simulated to peak temperatures of 893°C and 1088°C had much lower transition temperatures than the parent plate. This was attributed to a marked refinement of the structure. Simulation to a peak temperature of 788°C produced no marked effect on the transition temperature due to the fact that the large areas of ferrite had been visibly unaffected by the thermal cycle. Simulation to a peak temperature of 1347°C produced a slight increase in the transition temperature of the parent plate and this was associated with a coarse Widmanstätten structure of proeutectoid ferrite and upper bainite.

7. In Material B the proof stress, U.T.S. and hardness increased and the ductility decreased as the peak temperature of simulation increased to 1088°C. Above this temperature there was a slight drop in hardness and U.T.S. and an increase in ductility, although the proof stress continued to rise.

8. A simulated post-weld heat treatment in the temperature range 600°C - 645°C in Material B produced a marked increase in transition temperature in material simulated to peak temperatures of 1088°C and 1347°C. This was accompanied by an increase in hardness and proof stress. These changes in mechanical properties have been attributed to the occurrence of secondary hardening, due to the high V content of the material. A marked increase in transition temperature also occurred in material simulated to a peak temperature of 893°C and was accompanied by a drop in hardness and U.T.S. and an increase in ductility. These changes were associated with a softening of the structure, although the large increase in grain size had an over-riding effect in increasing the transition temperature. Material simulated to a peak temperature of 788°C had improved tensile and Charpy V-notch-impact properties after the simulated post-weld heat treatment. This was attributed to a tempering effect on the transformation products of high carbon austenite resulting from the weld thermal cycle.

9. Secondary hardening measurements on material simulating the grain coarsened region of the weld HAZ, in the temperature range 500°C - 700°C, indicated that maximum hardening occurred in the temperature range normally recommended for post-weld heat treatment in this type of material. To overcome this the temperature should be in the range 675°C - 700°C.

10. Tensile tests on Material A simulated through weld thermal cycles with peak temperatures in the range 200°C - 656°C showed that a very slight increase in strength and decrease in ductility occurs above about 300°C. However, the effects of stress-raisers and the restraint of surrounding material has been neglected in this approach.

6. Bibliography

1. "Fabricating 140 ton boiler drums", Weld. and Met. Fab., 34 (1) 1966, p.4.

2. McKenzie, I.M., Chem. & Proc. Eng. April 1959, p.132.

3. Nicholls, D.M., D.A.E. Thesis, College of Aeronautics, 1966.

4. B.W.R.A. Bulletin 7 (6), 1966.

5. George, M.J. and Clifton, T.E., Materials Department, College of Aeronautics Note No. 15, Cranfield.

6. Smith, E., Coward, M.D., and Apps, R.L., College of Aeronautics Report Mat. No. 2, Cranfield, 1968.

7. Coward, M.D. and Apps, R.L., College of Aeronautics Note Mat. No. 13, Cranfield, 1967.

8. Andrews, K.W., J.I.S.I. 203, (7) 1965, p.721.

9. Albutt, K.J. and Garber, S., J.I.S.I. 204, (12) 1966, p.1217.

10. Petch, N.J., Phil. Mag. 3, 1958, p.1089.

11. Heslop, J. and Petch, N.J., Phil. Mag. 3, 1958, p.1128.

12. Irvine, K.J. and Pickering, F.B., J.I.S.I., 188, 1958, p.101.

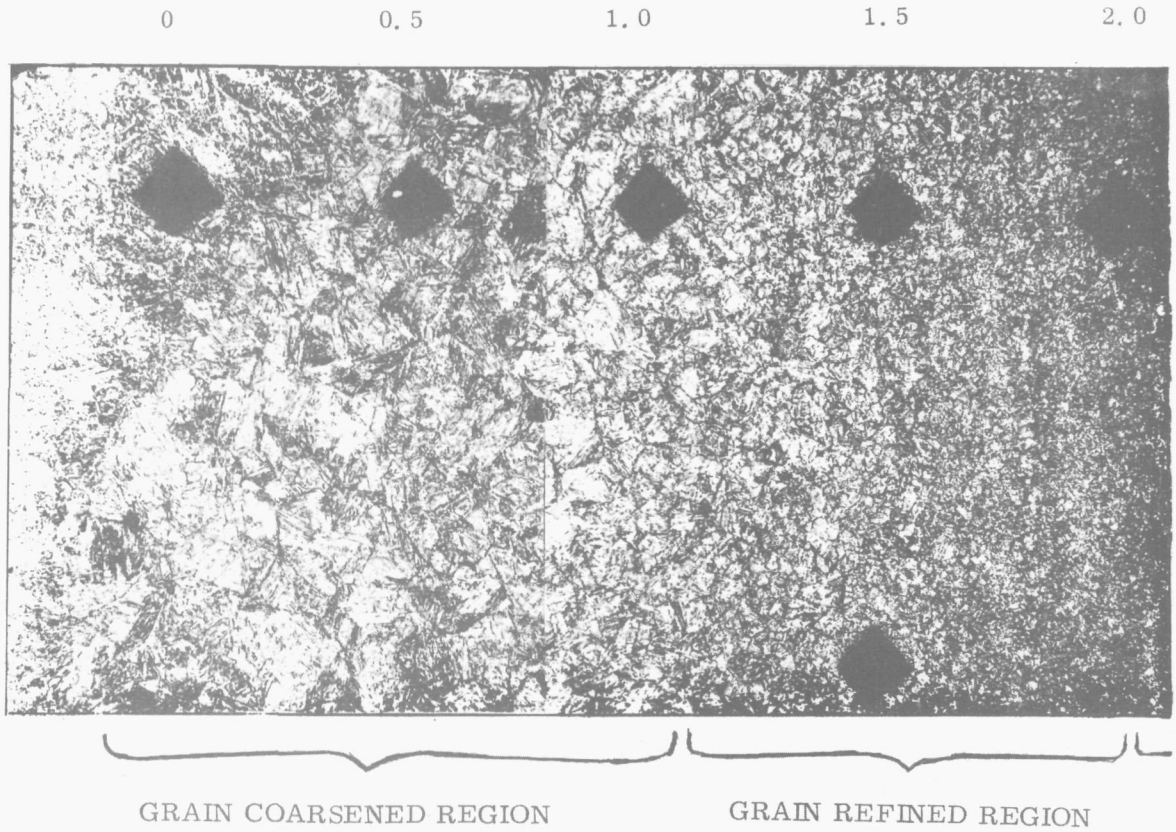

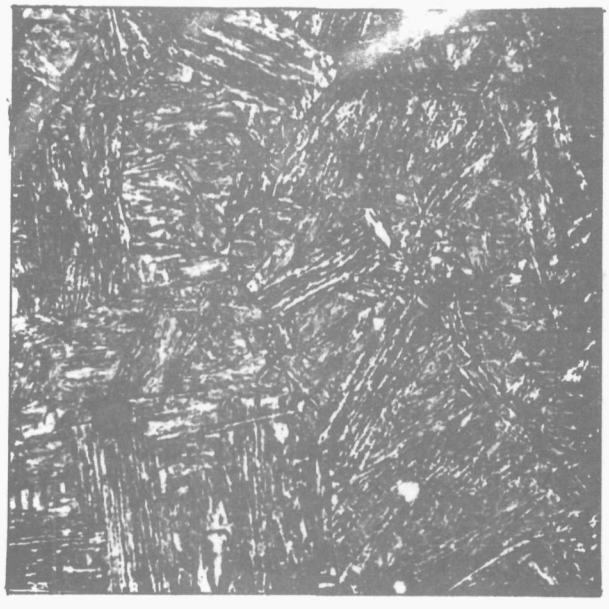

(A) GRAIN COARSENED REGION x500

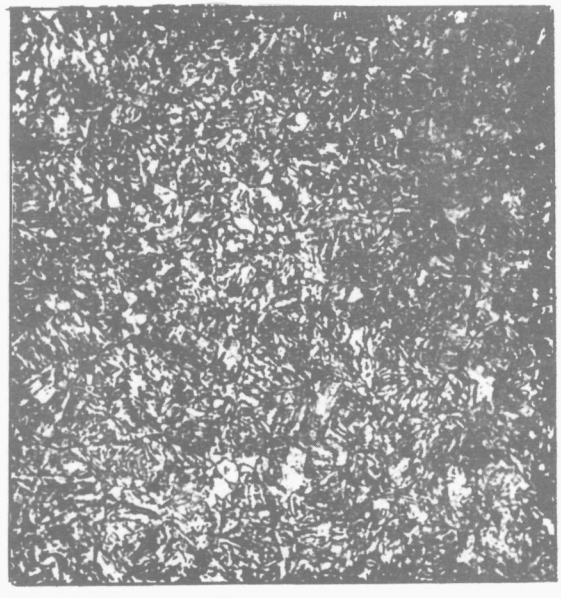

(B) GRAIN REFINED REGION x500

FIG. 1 MATERIAL 'A' - WELD HEAT AFFECTED ZONE MICROSTRUCTURES

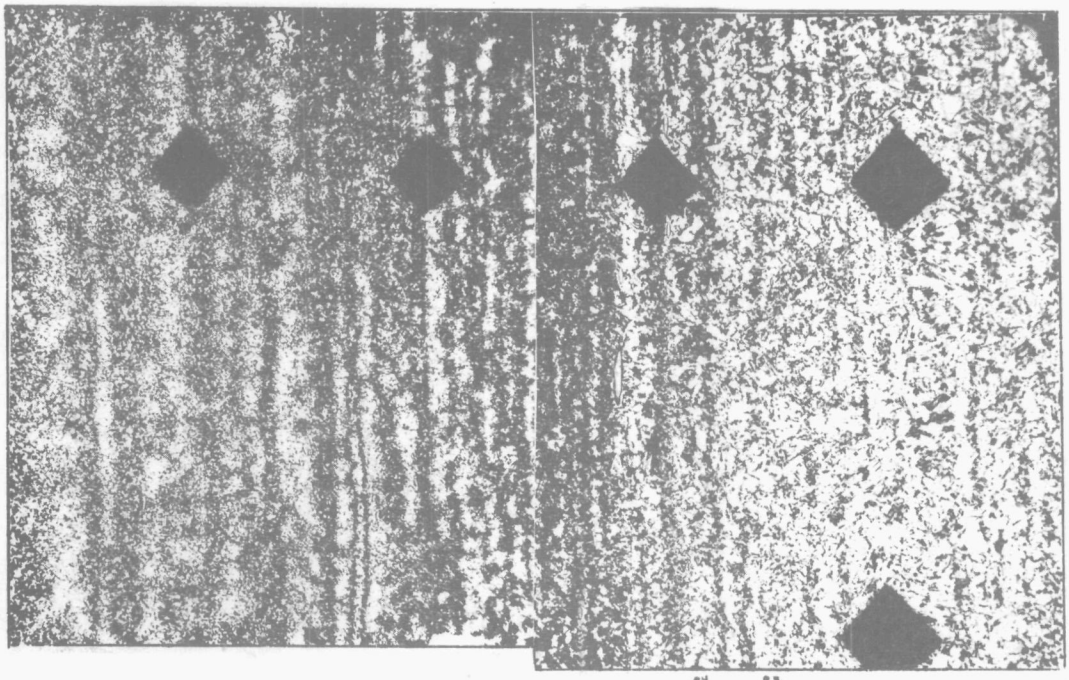

x70

PARTIAL TRANSFORMATION REGION

SPHERIODISED REGION

PARENT PLATE

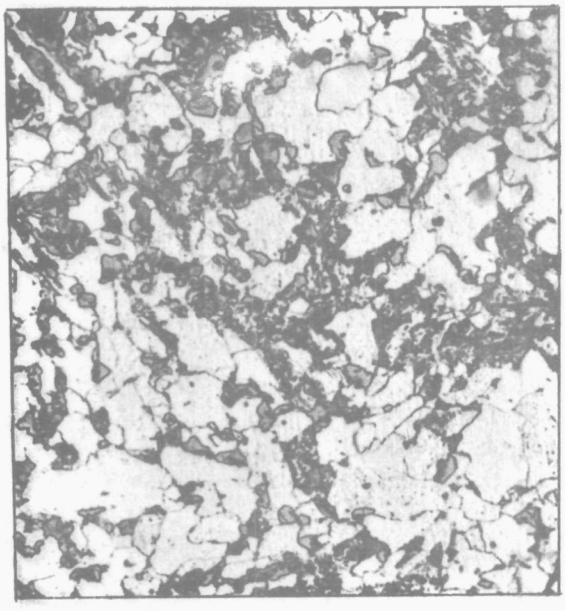

(C) PARTIAL TRANSFORMATION REGION x500

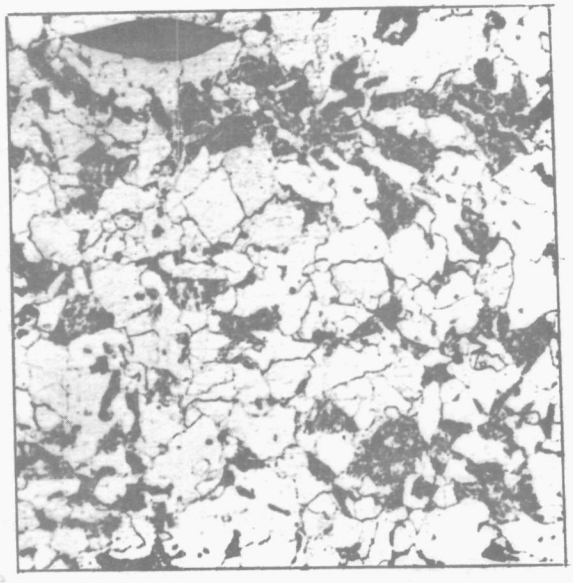

(D) PARENT PLATE x500

FIG. 1 MATERIAL 'A' (continued)

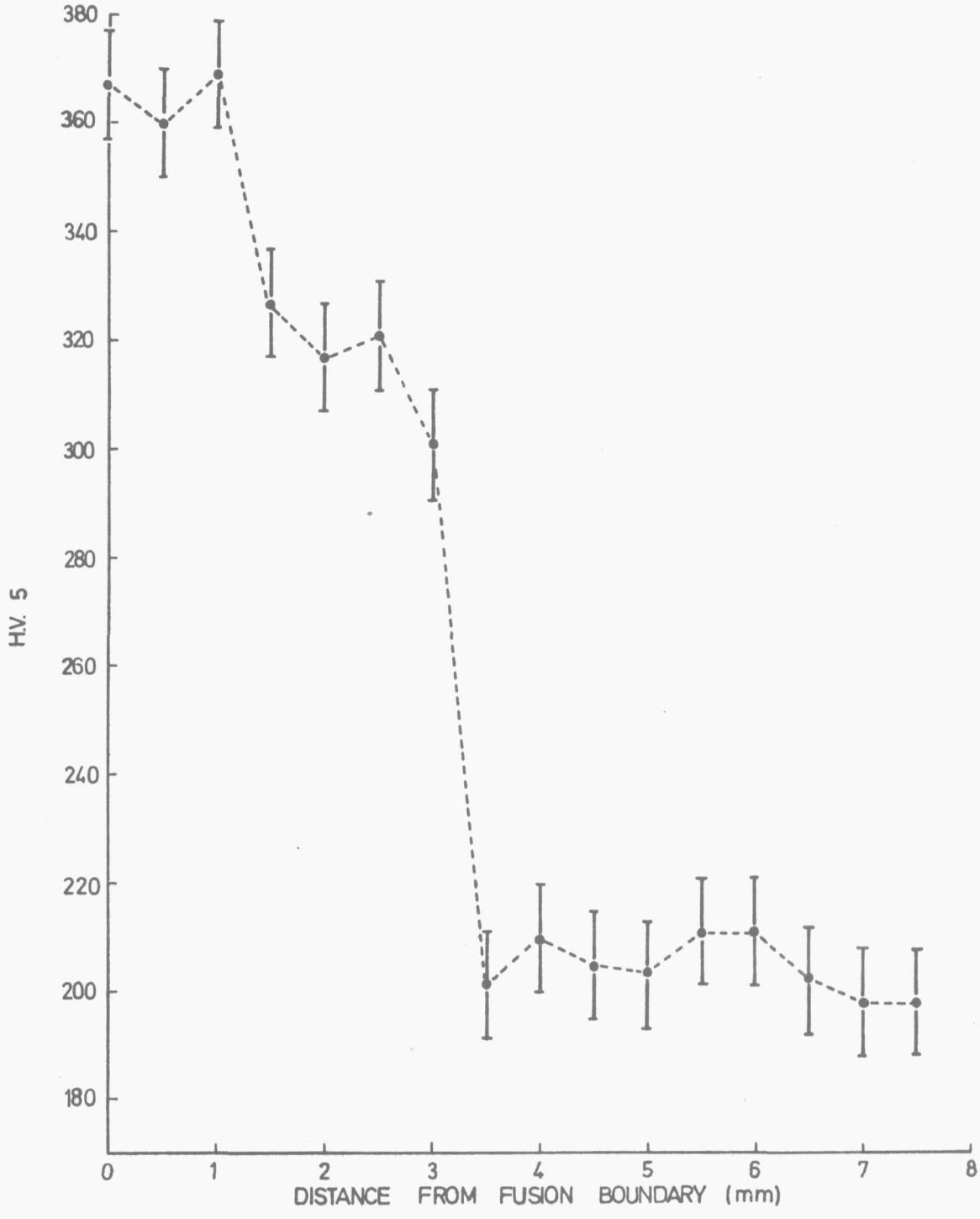

FIG. 2 DUCOL W30 HEAT AFFECTED ZONE HARDNESS SURVEY. (MATERIAL A)

OPTICAL MICROGRAPH

x500

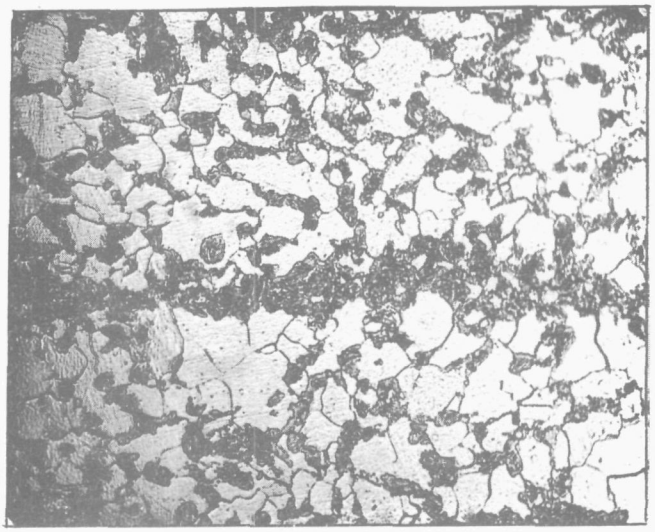

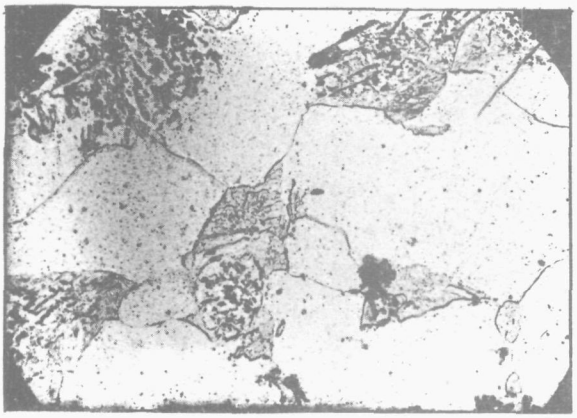

ELECTRON MICROGRAPH

x4, 000

ELECTRON MICROGRAPH

x30, 000

HV 10 = 214 $\pm$ 10

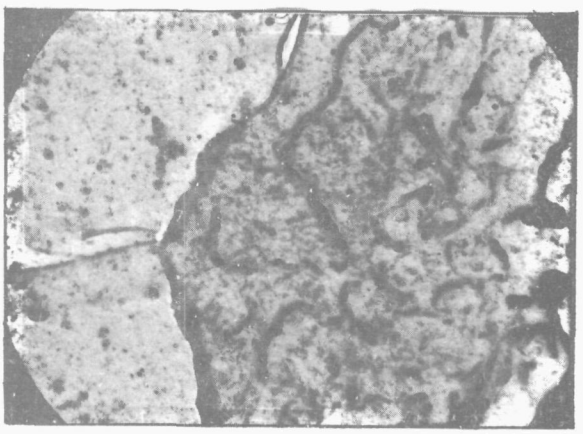

FIG. 3 PHOTOMICROGRAPHS OF MATERIAL 'A' AFTER SIMULATION TO A PEAK TEMPERATURE OF 788^{o}C

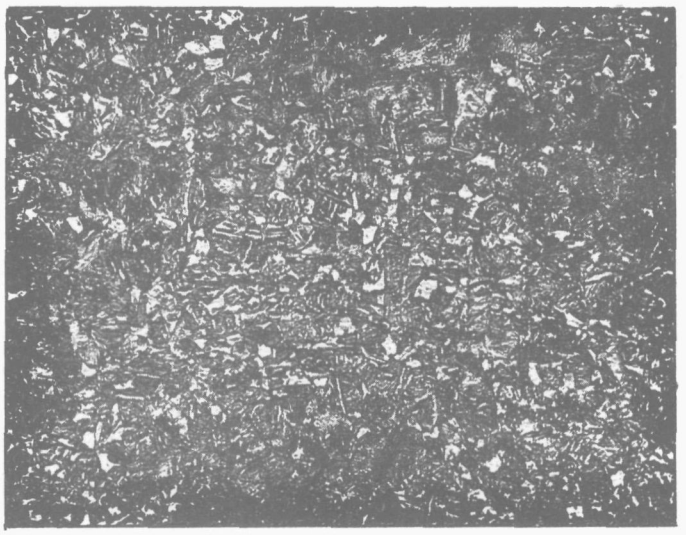

OPTICAL MICROGRAPH x500

HV 10 = 341 $\pm$ 10

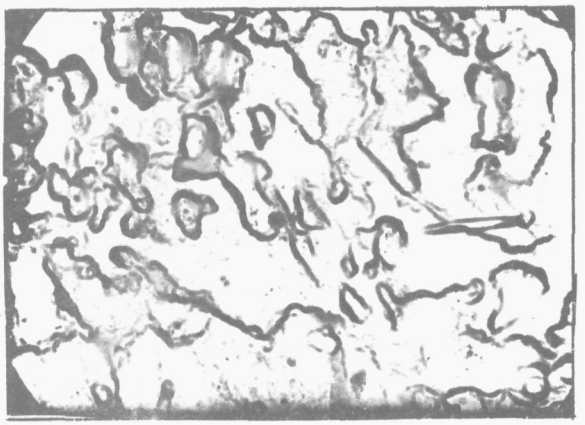

ELECTRON MICROGRAPH x15, 000

FIG. 4 PHOTOMICROGRAPHS OF MATERIAL 'A' AFTER SIMULATION TO A PEAK TEMPERATURE OF 893^{o}C

OPTICAL MICROGRAPH

x500

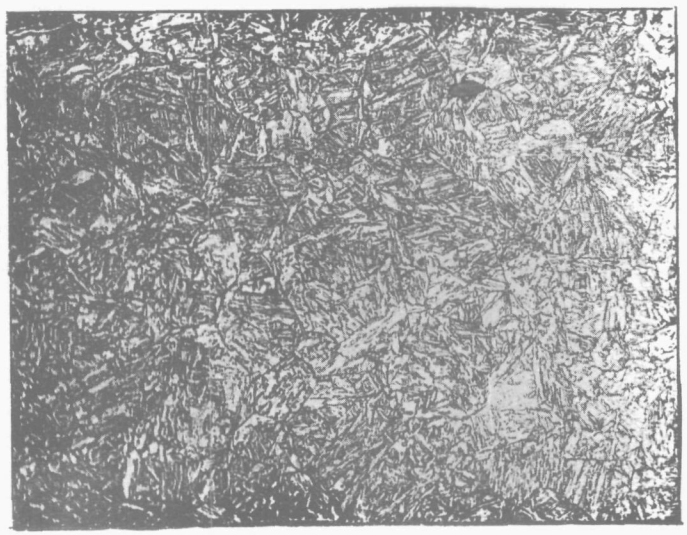

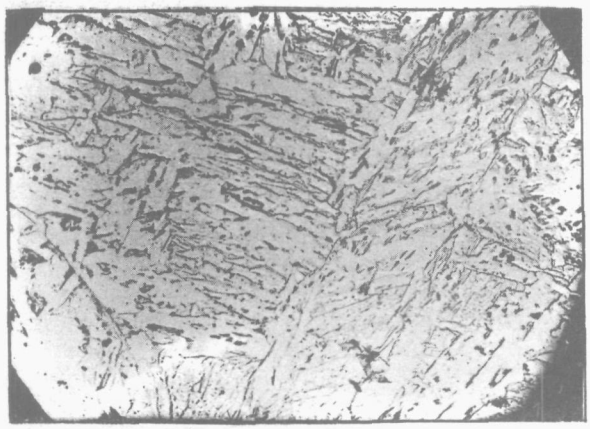

ELECTRON MICROGRAPH

x4, 000

ELECTRON MICROGRAPH

x30, 000

HV 10 = 310 $\pm$ 10

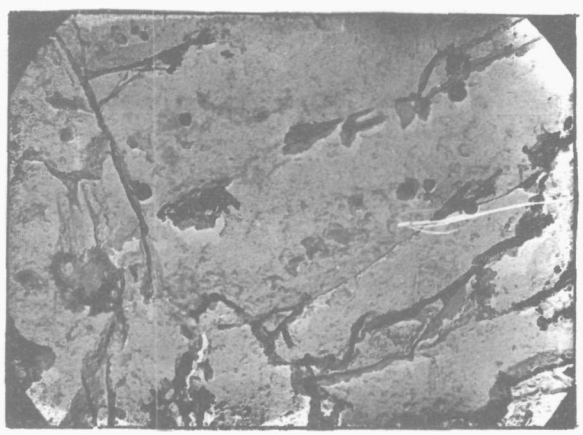

FIG. 5 PHOTOMICROGRAPHS OF MATERIAL 'A' AFTER SIMULATION TO A PEAK TEMPERATURE OF 1088^{o}C

OPTICAL MICROGRAPH

x500

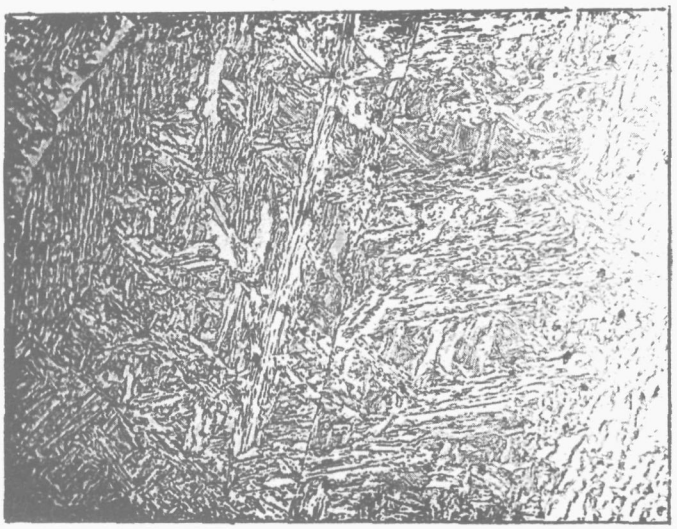

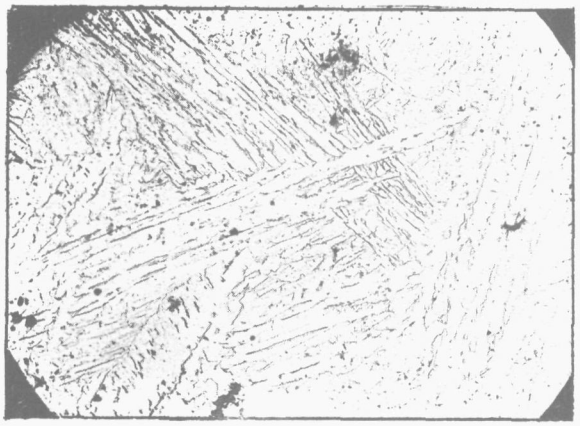

ELECTRON MICROGRAPH

x4, 000

ELECTRON MICROGRAPH

x33, 000

HV 10 = 298 $\pm$ 10

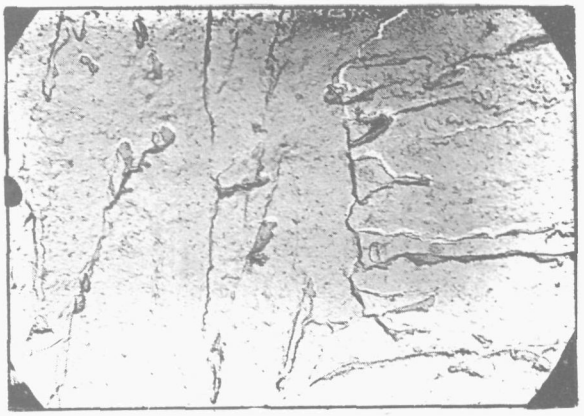

FIG. 6 PHOTOMICROGRAPHS OF MATERIAL 'A' AFTER SIMULATION TO A PEAK TEMPERATURE OF 1347^{o}C

OPTICAL MICROGRAPH

x500.

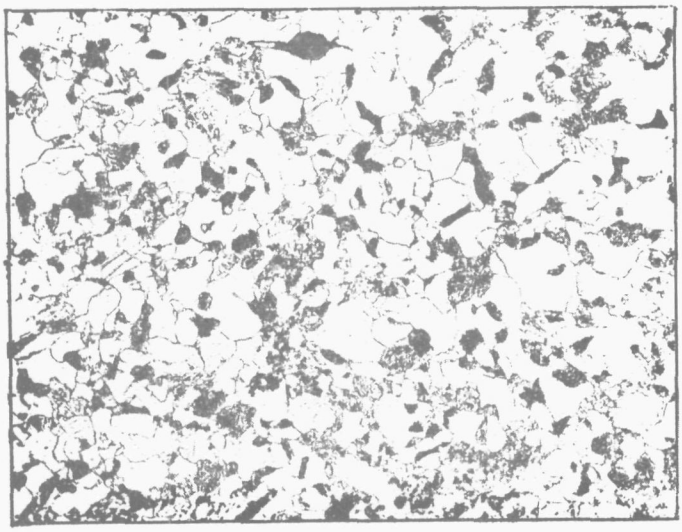

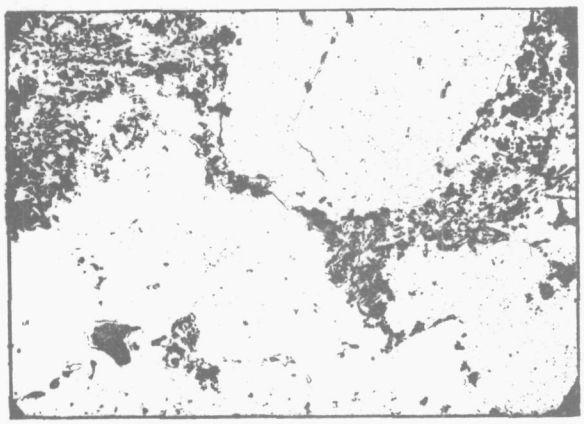

ELECTRON MICROGRAPH

x3, 000

ELECTRON MICROGRAPH

x13, 000

HV 10 = 196 ± 10

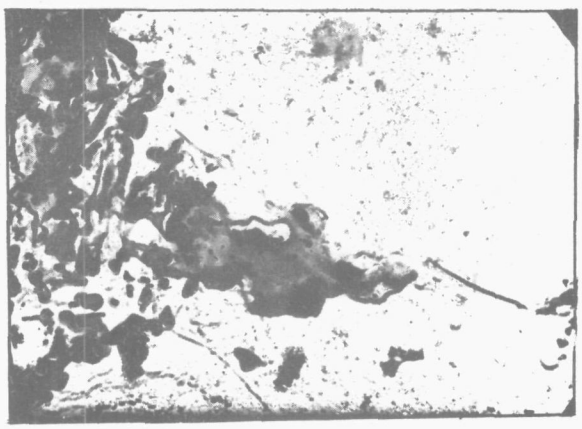

FIG. 7 PHOTOMICROGRAPHS OF MATERIAL 'A' PARENT PLATE

OPTICAL MICROGRAPH

x1, 000

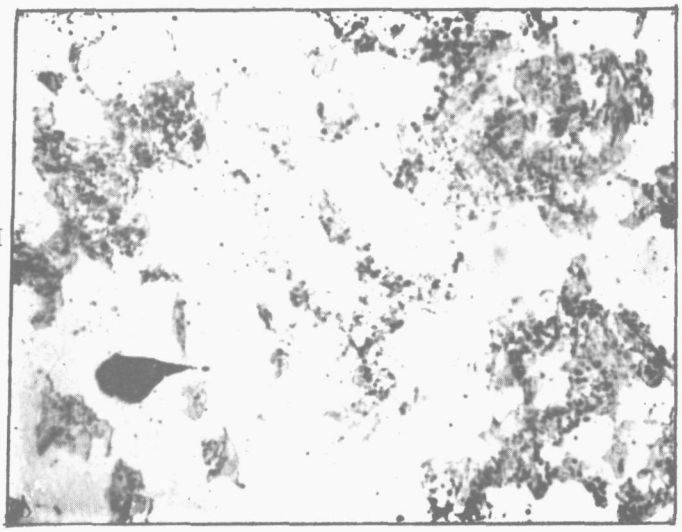

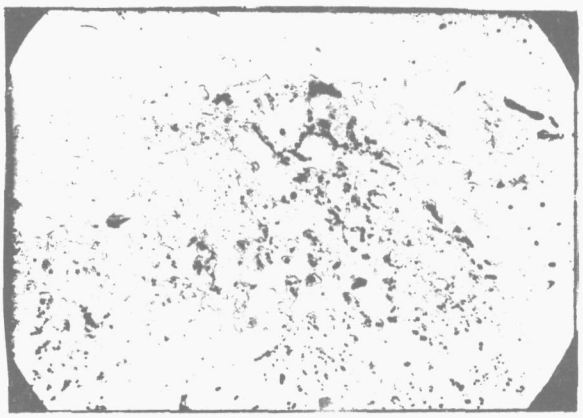

ELECTRON MICROGRAPH

x6, 000

ELECTRON MICROGRAPH

x28, 000

HV 10 = 234 $\pm$ 10

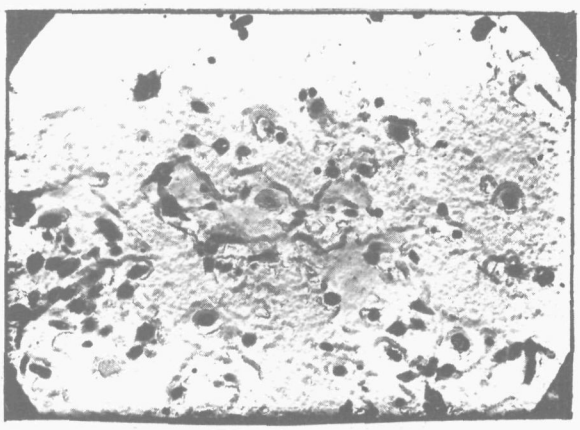

FIG. 8 PHOTOMICROGRAPHS OF MATERIAL 'B' AFTER SIMULATION TO A PEAK TEMPERATURE OF 788^{o}C

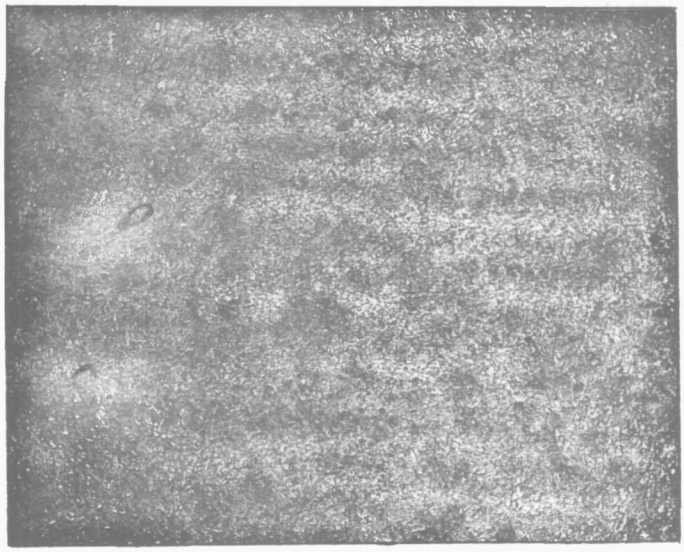

OPTICAL MICROGRAPH x100

HV 10 = 276 $\pm$ 10

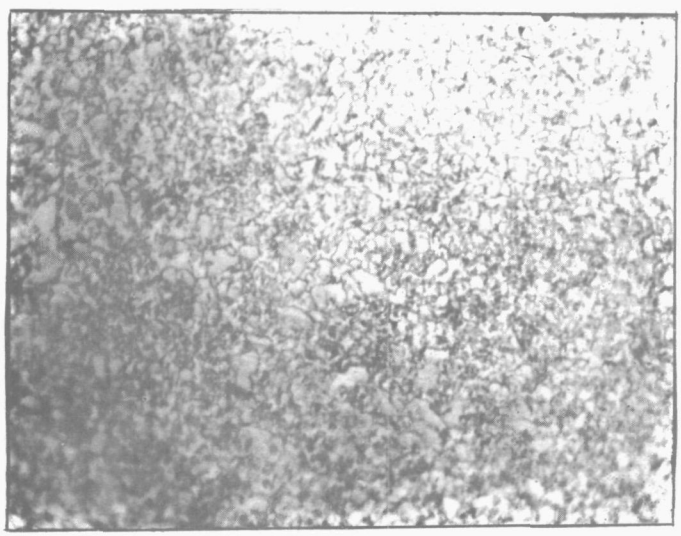

OPTICAL MICROGRAPH x1, 000

FIG. 9 PHOTOMICROGRAPHS OF MATERIAL 'B' AFTER SIMULATION TO A PEAK TEMPERATURE OF 893^{o}C

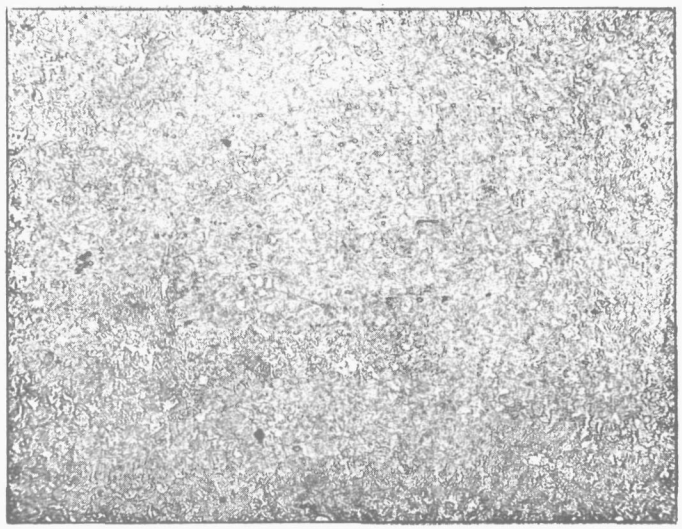

OPTICAL MICROGRAPH x100

HV10 = 288 $\pm$ 10

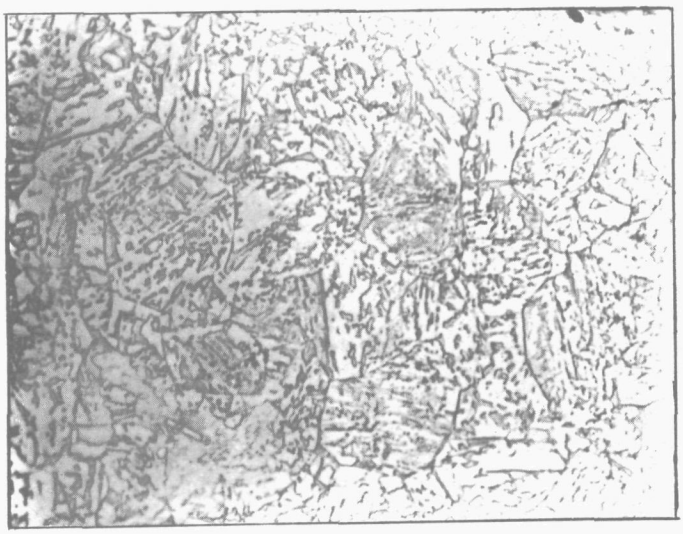

OPTICAL MICROGRAPH x1, 000

FIG. 10 PHOTOMICROGRAPHS OF MATERIAL 'B' AFTER SIMULATION TO A PEAK TEMPERATURE OF 1088^{o}C

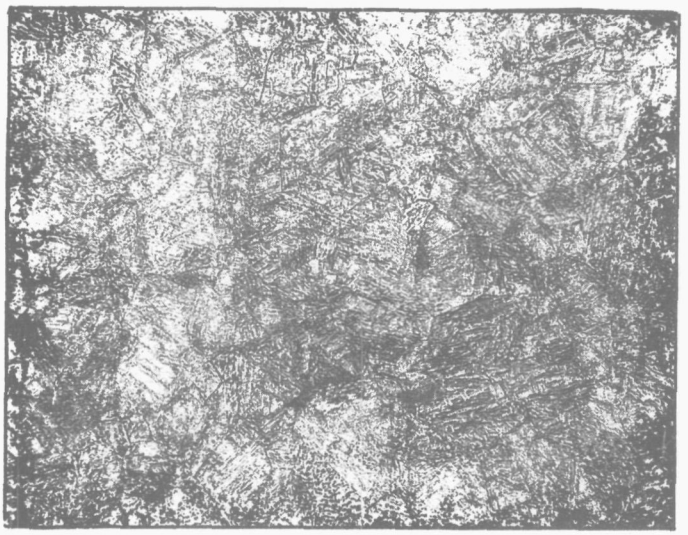

OPTICAL MICROGRAPH x100

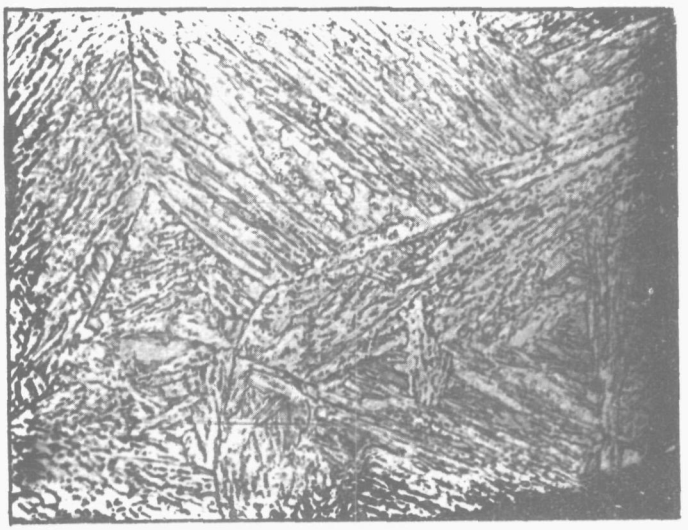

HV 10 = 281 $\pm$ 10

OPTICAL MICROGRAPH x1, 000

FIG. 11 PHOTOMICROGRAPHS OF MATERIAL 'B' AFTER SIMULATION TO A PEAK TEMPERATURE OF 1347^{o}C

OPTICAL MICROGRAPH

x1000

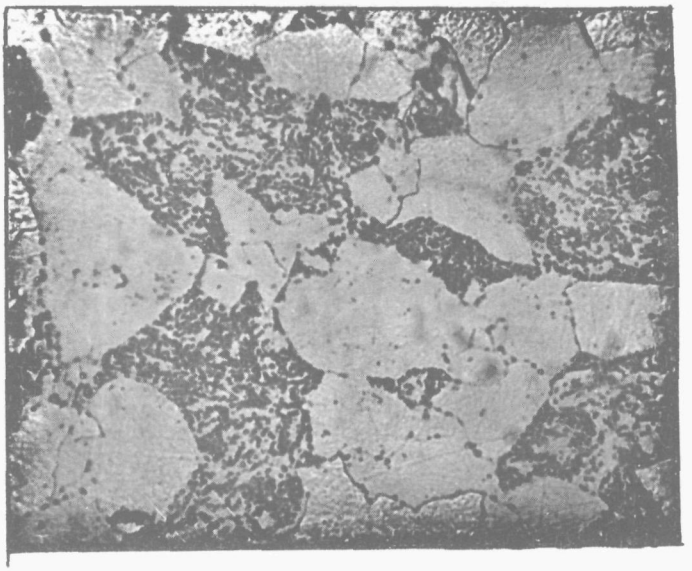

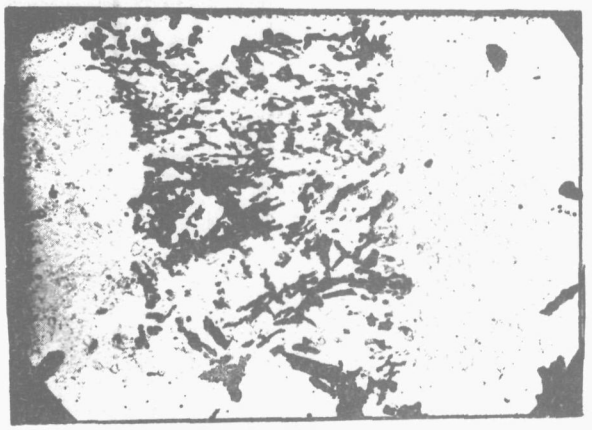

ELECTRON MICROGRAPH

x6000

ELECTRON MICROGRAPH

x28, 000

HV 10 = 200 $\pm$ 10

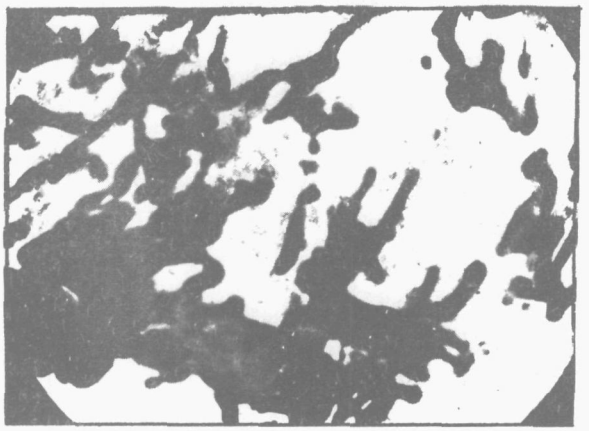

FIG. 12 PHOTOMICROGRAPHS OF MATERIAL 'B' PARENT PLATE

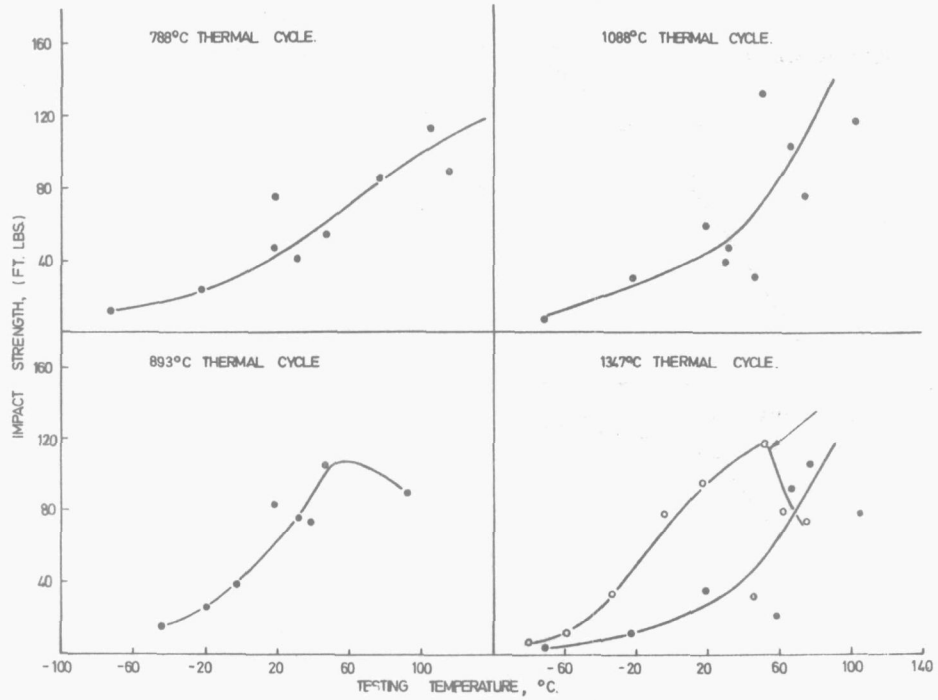

FIG. 13 CHARPY V-NOTCH IMPACT (FT. LBS) TEMPERATURE DATA FOR DUCOL W30 SIMULATED SPECIMENS (MATERIAL A)

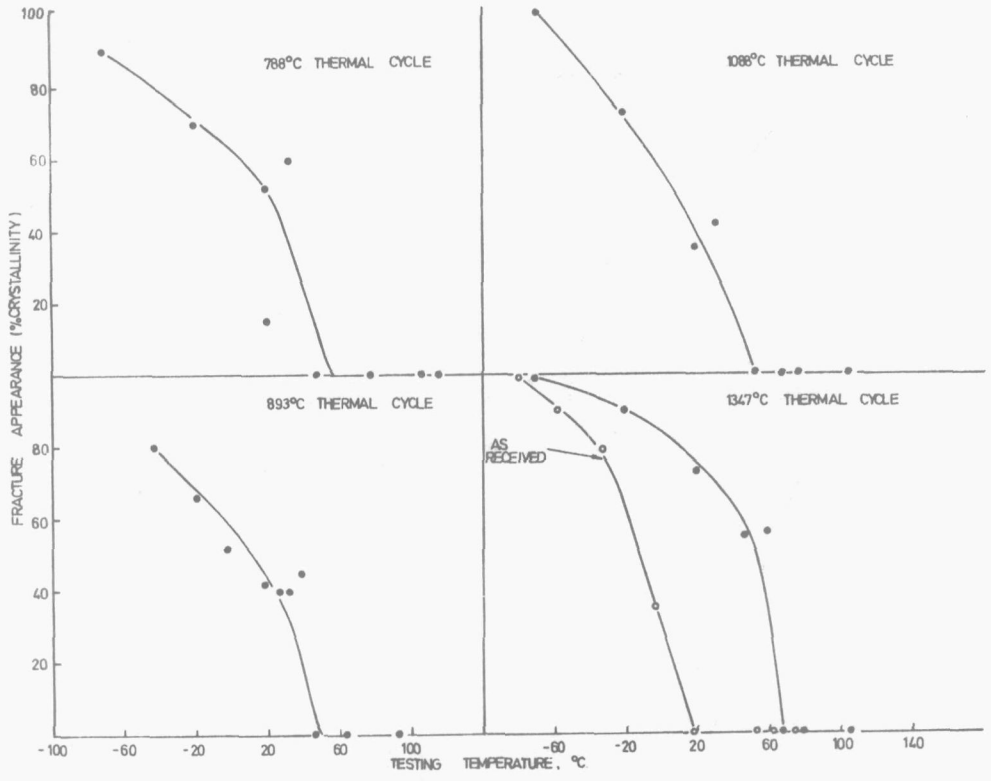

FIG. 14 CHARPY V-NOTCH IMPACT (% CRYSTALLINITY)- TEMPERATURE DATA FOR DUCOL W30 SIMULATED SPECIMENS (MATERIAL A)

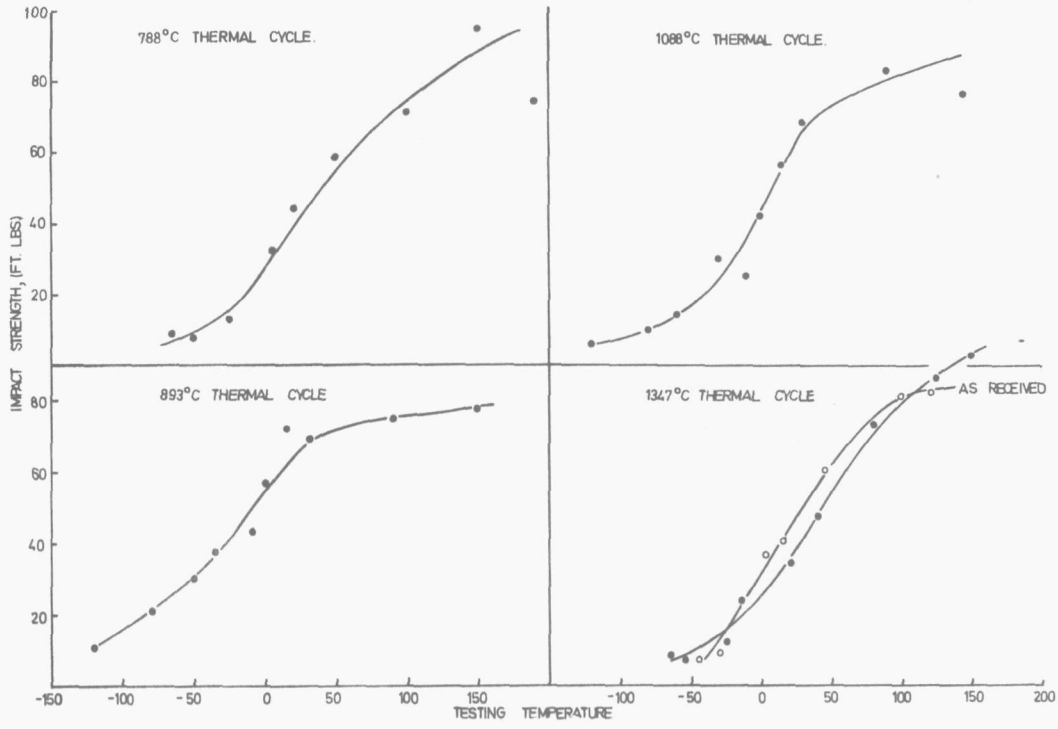

FIG. 15 CHARPY V-NOTCH IMPACT (FT. LBS.) TEMPERATURE DATA FOR DUCOL BW87A SIMULATED SPECIMENS (MATERIAL B)

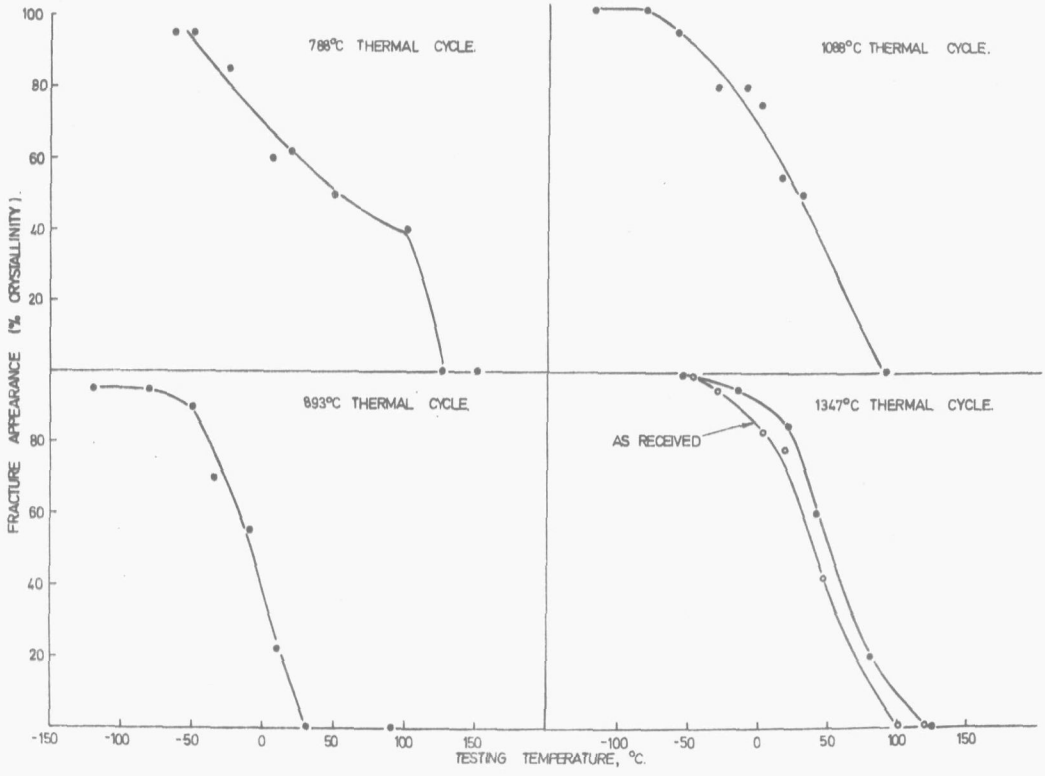

FIG. 16 CHARPY V-NOTCH IMPACT (% CRYSTALLINITY) TEMPERATURE DATA FOR DUCOL BW 87A SIMULATED SPECIMENS (MATERIAL B)

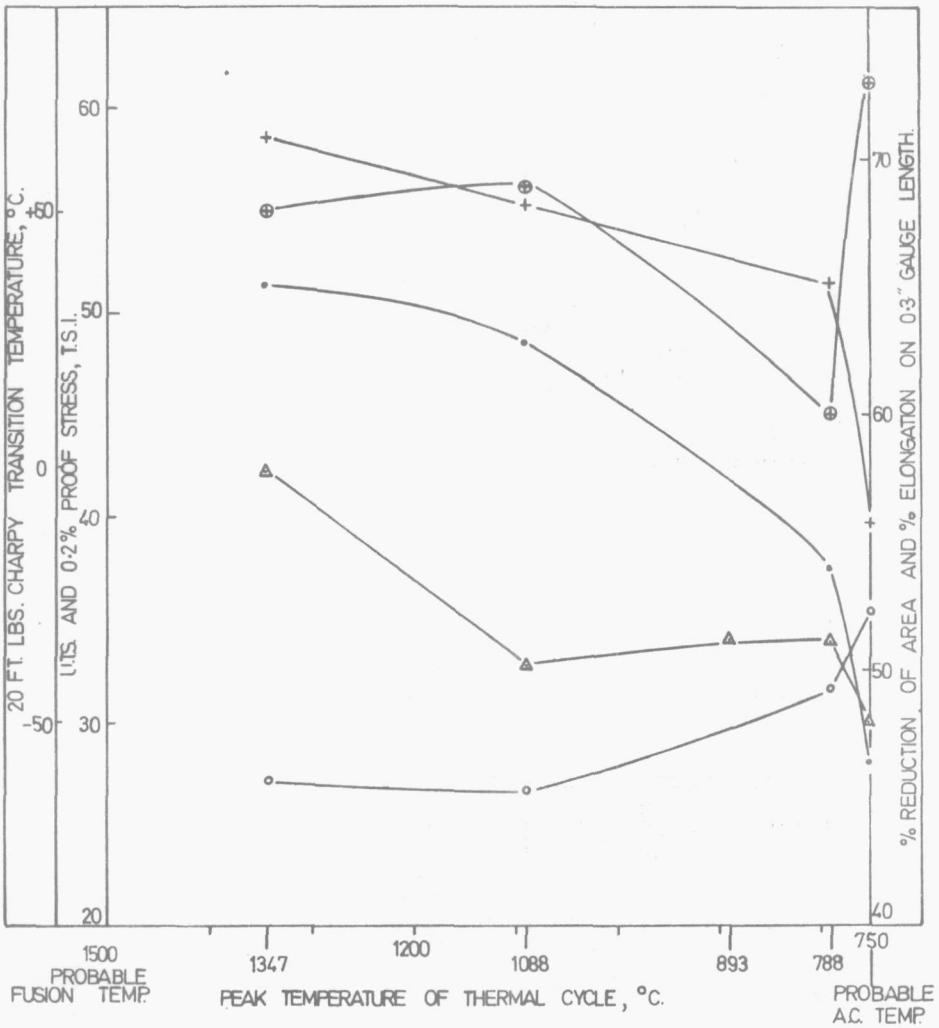

FIG. 17 MECHANICAL PROPERTIES OF SIMULATED H.A.Z. STRUCTURES IN DUCOL W30 (MATERIAL A)

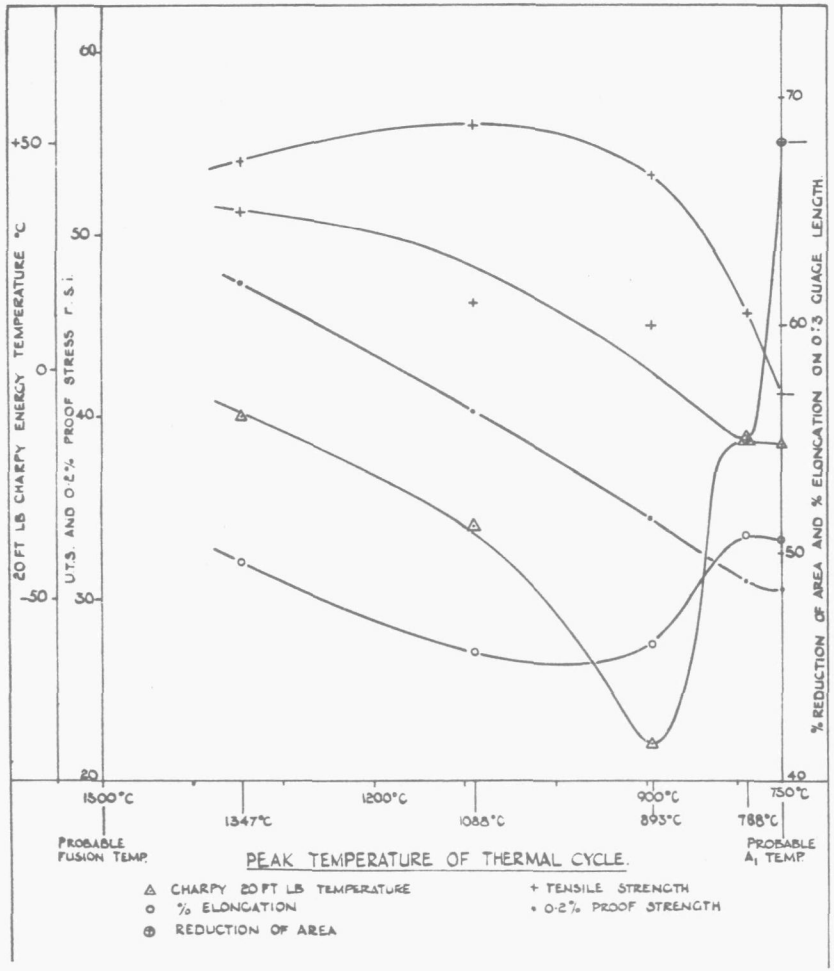

FIG. 18 MECHANICAL PROPERTIES OF SIMULATED H.A.Z. STRUCTURES (MATERIAL B)

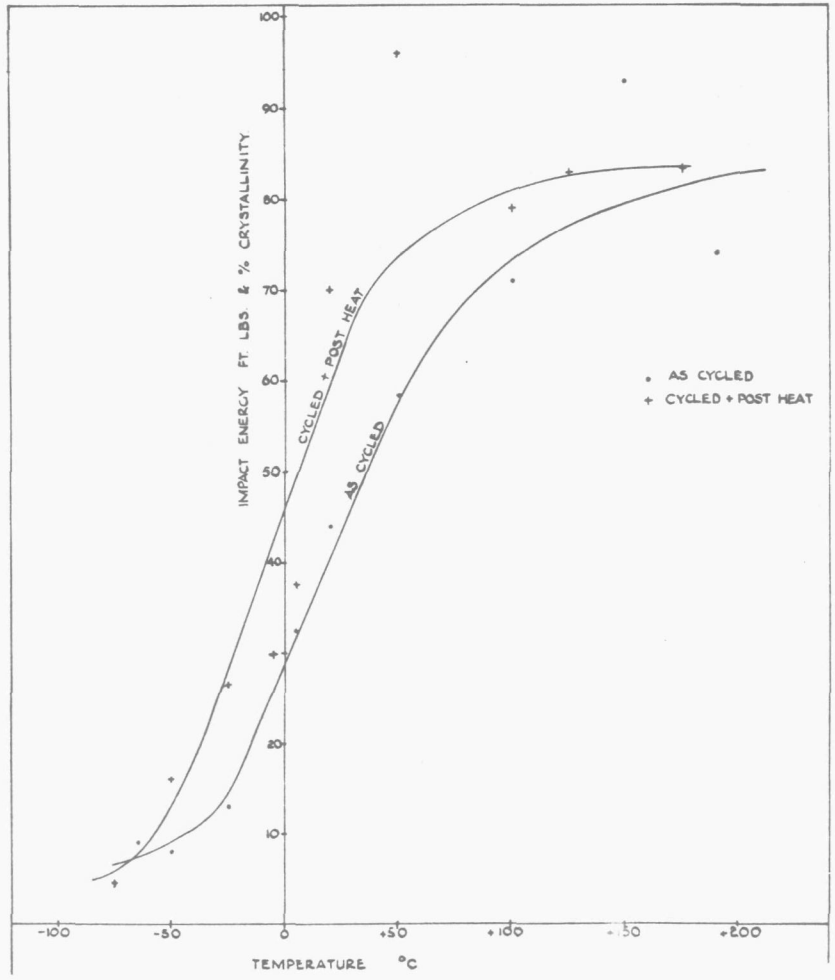

FIG. 19 CHARPY TRANSITION CURVES FOR 788°C PEAK TEMPERATURE (MATERIAL B)

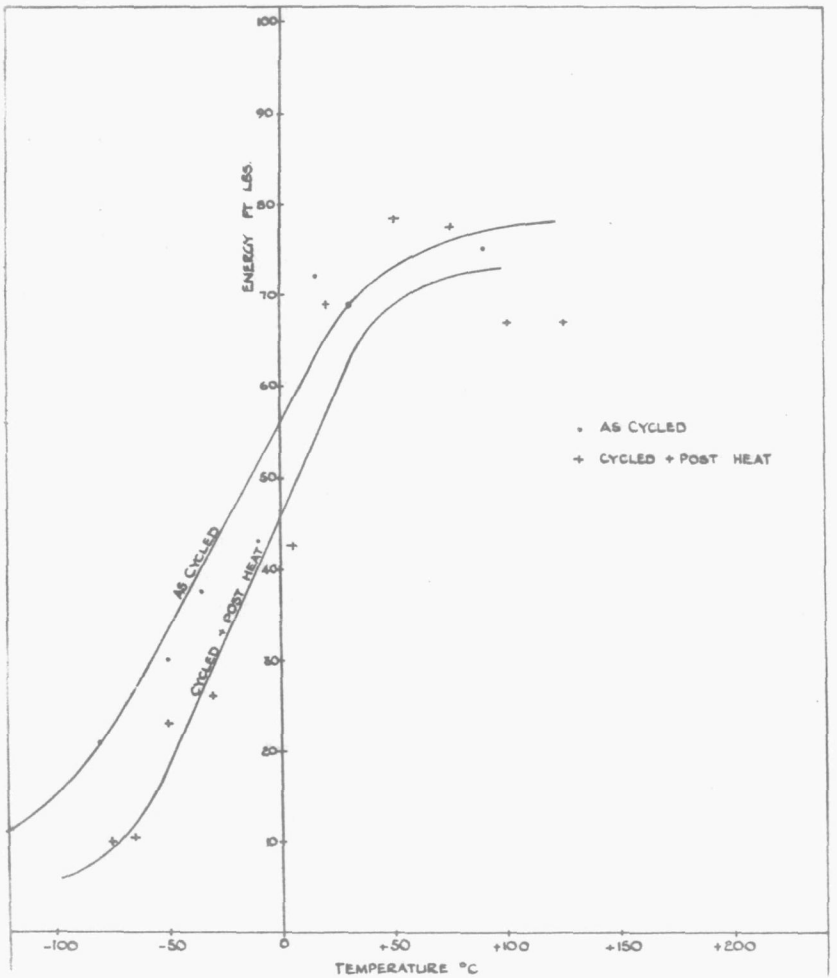

FIG. 20 CHARPY TRANSITION CURVES FOR 893°C PEAK TEMPERATURE (MATERIAL B)

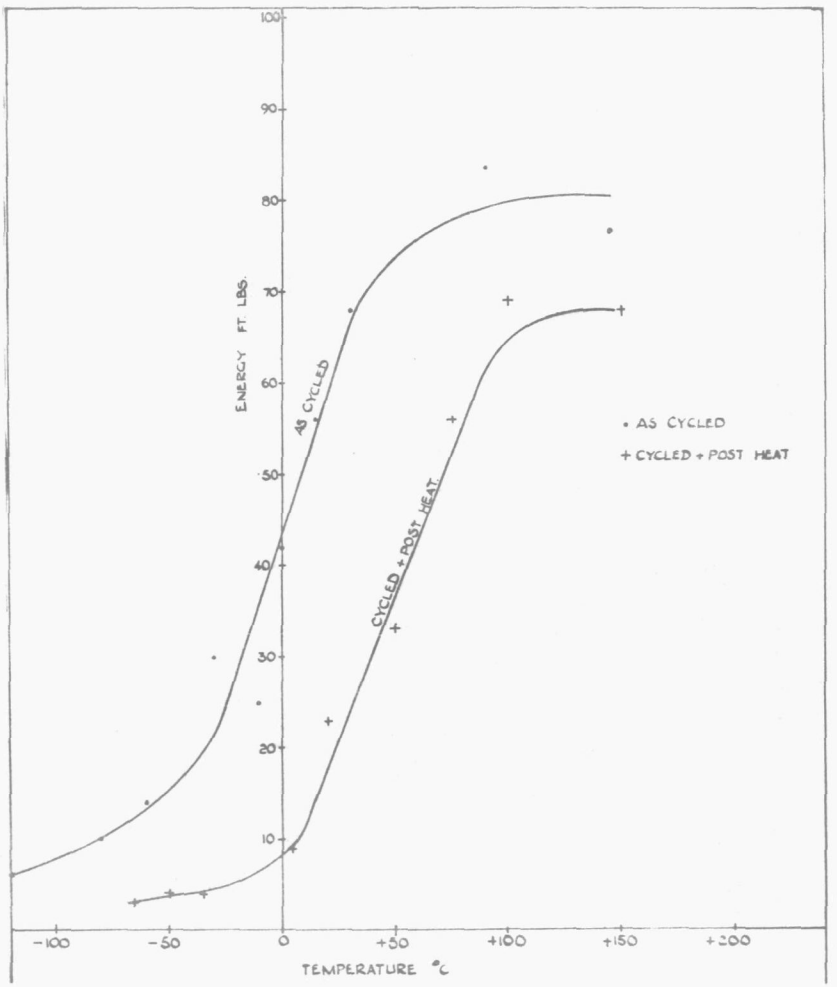

FIG. 21 CHARPY TRANSITION CURVES FOR 1088°C PEAK TEMPERATURE (MATERIAL B)

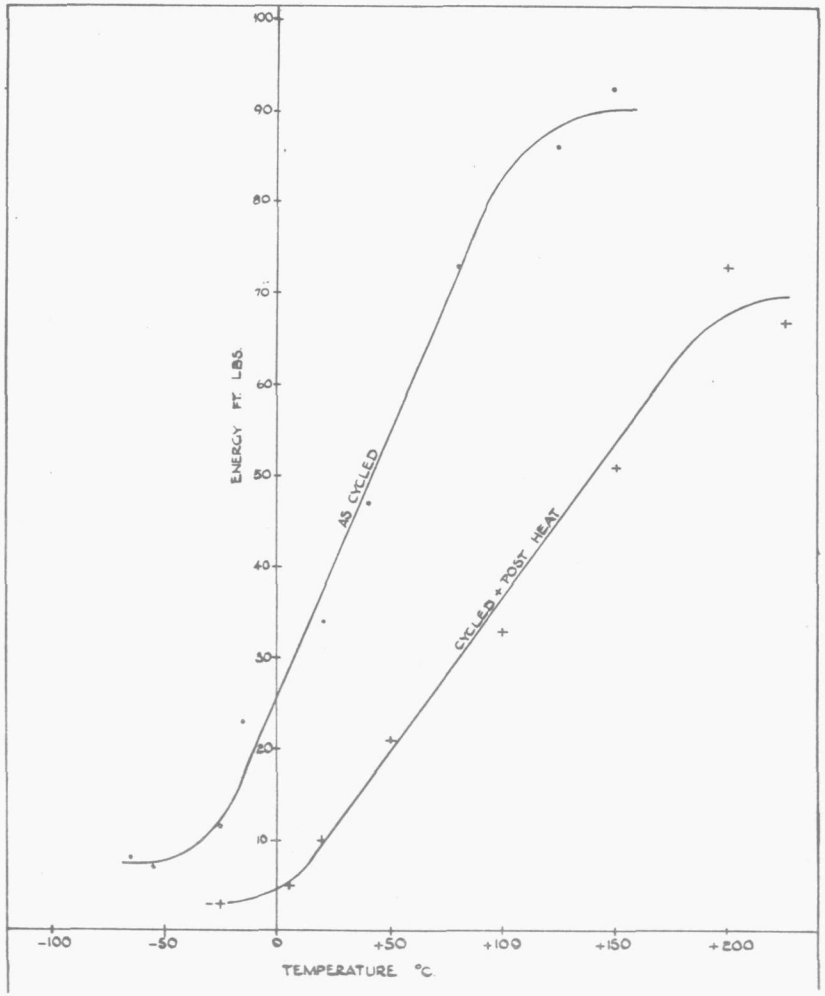

FIG. 22 CHARPY TRANSITION CURVES FOR 1347°C PEAK TEMPERATURE (MATERIAL B)

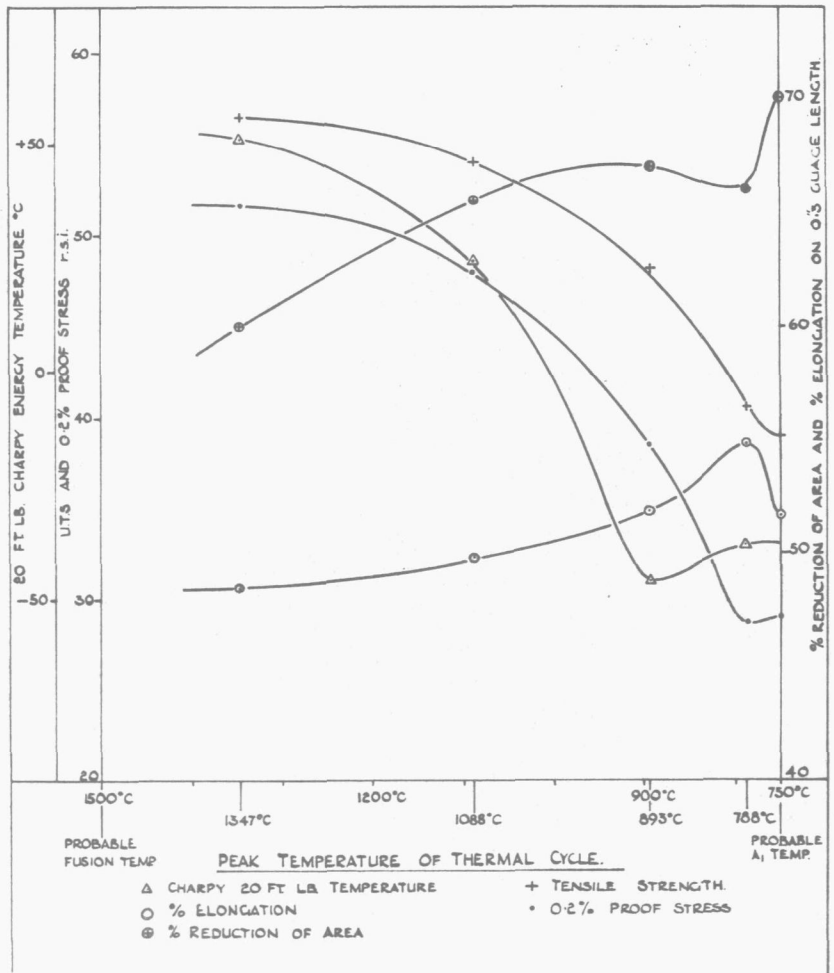

FIG. 23 MECHANICAL PROPERTIES OF SIMULATE H.A.Z. STRUCTURES AFTER POST WELD HEAT TREATMENT (MATERIAL B)

OPTICAL MICROGRAPH

x1000

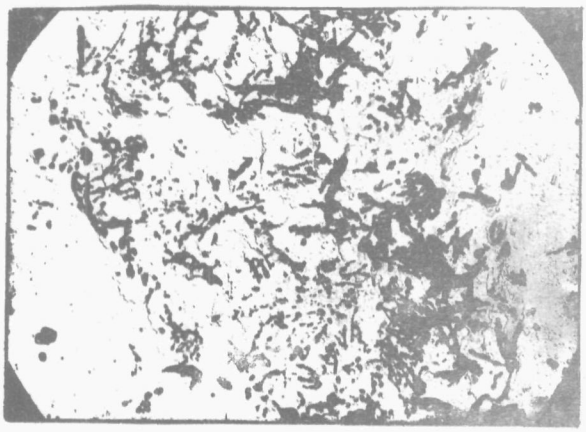

ELECTRON MICROGRAPH

x6000

ELECTRON MICROGRAPH

x28,000

HV 10 = 198 $\pm$ 10

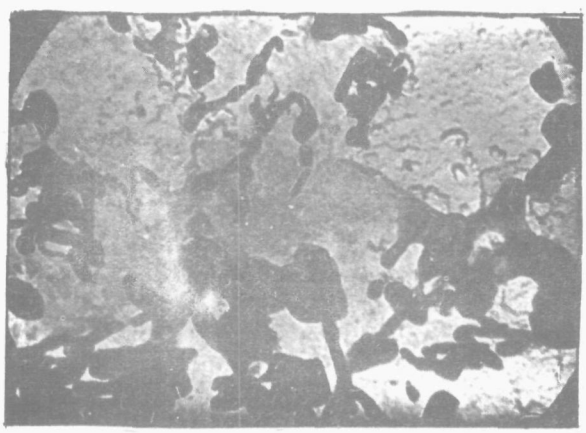

FIG. 24 PHOTOMICROGRAPHS OF MATERIAL 'B' PARENT PLATE AFTER SIMULATED POST WELD HEAT TREATMENT

OPTICAL MICROGRAPH

x1000

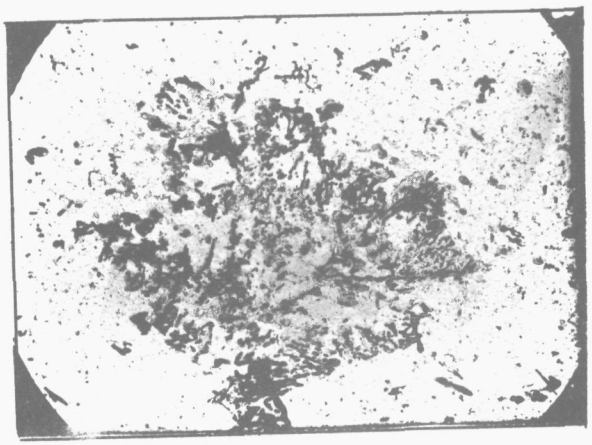

ELECTRON MICROGRAPH

x6000

ELECTRON MICROGRAPH

X28, 000

HV 10 = 200 $\pm$ 10

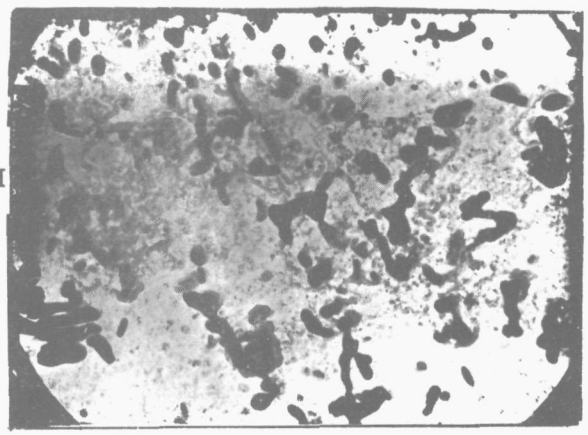

FIG. 25 PHOTOMICROGRAPHS OF MATERIAL 'B' SIMULATED TO A PEAK TEMPERATURE OF 788^{o}C AND POST WELD HEAT TREATED

OPTICAL MICROGRAPH

x1, 000

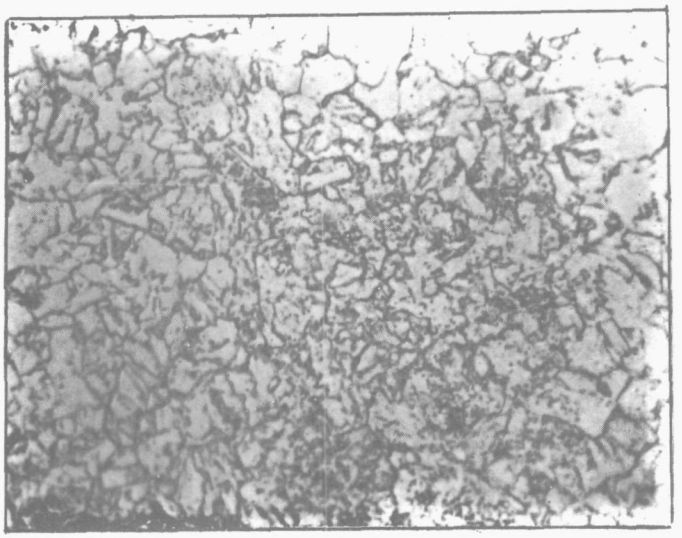

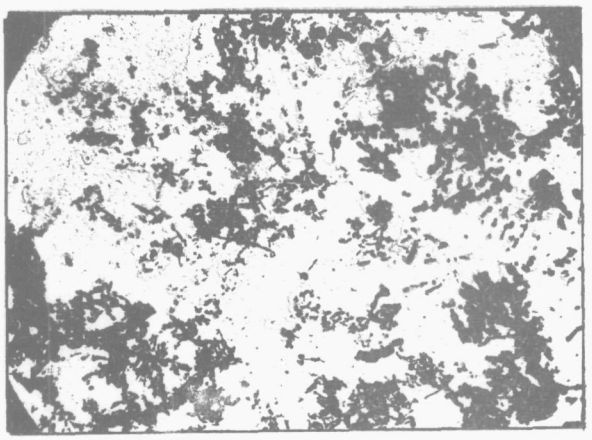

ELECTRON MICROGRAPH

x6, 000

ELECTRON MICROGRAPH

x28, 000

HV 10 = 261 $\pm$ 10

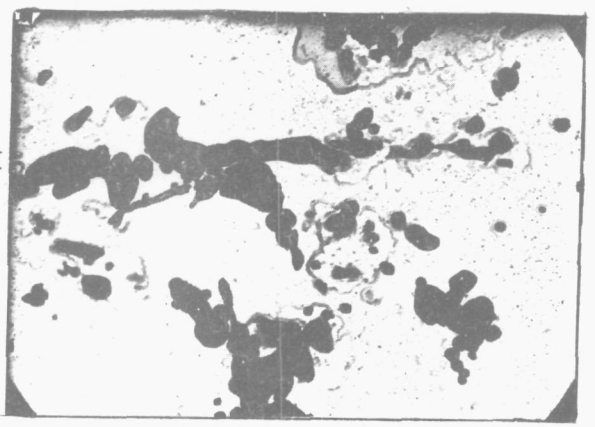

FIG. 26 PHOTOMICROGRAPHS OF MATERIAL 'B' SIMULATED TO A PEAK TEMPERATURE OF 893°C FOLLOWED BY SIMULATED POST WELD HEAT TREATMENT

OPTICAL MICROGRAPH

x1000

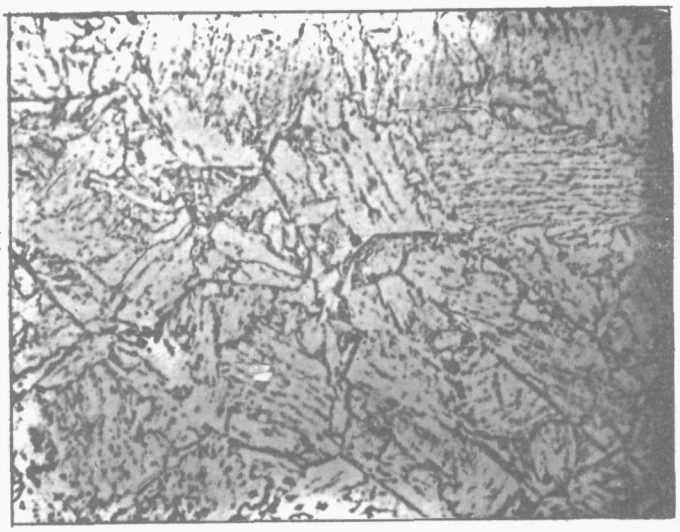

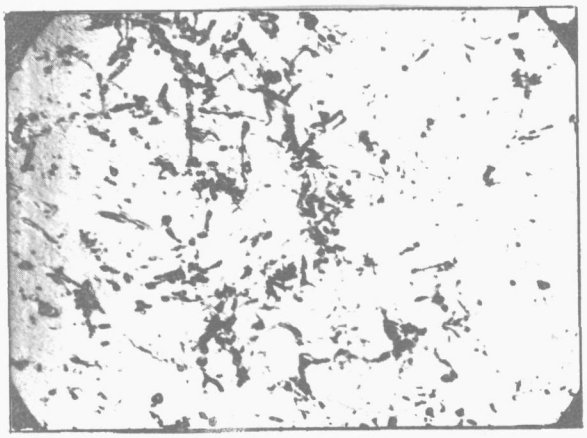

ELECTRON MICROGRAPH

x6, 000

ELECTRON MICROGRAPH

x28, 000

HV 10 = 300 $\pm$ 10

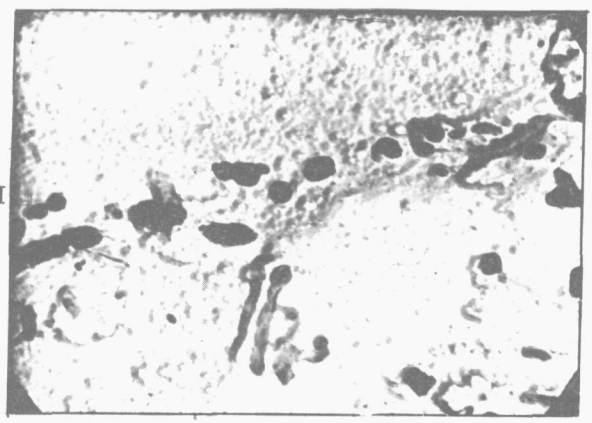

FIG. 27 PHOTOMICROGRAPHS OF MATERIAL 'B' SIMULATED TO A PEAK TEMPERATURE OF 1088^{o}C FOLLOWED BY SIMULATED POST WELD HEAT TREATMENT

OPTICAL MICROGRAPH

x1000

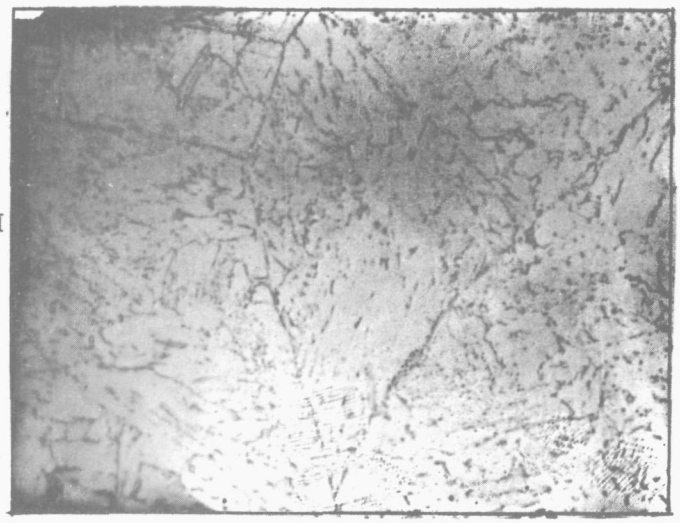

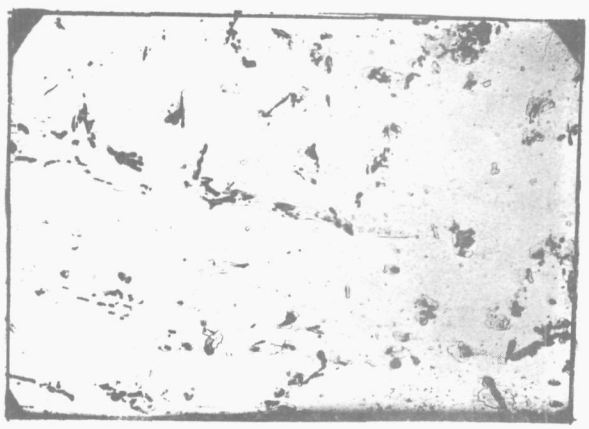

ELECTRON MICROGRAPH

x6, 000

ELECTRON MICROGRAPH

x28, 000

HV 10 = 295 $\pm$ 10

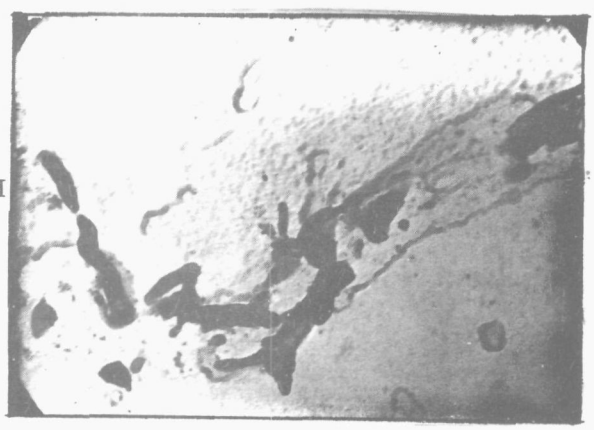

FIG. 28 PHOTOMICROGRAPHS OF MATERIAL 'B' SIMULATED TO A PEAK TEMPERATURE OF 1347°C FOLLOWED BY SIMULATED POST WELD HEAT TREATMENT

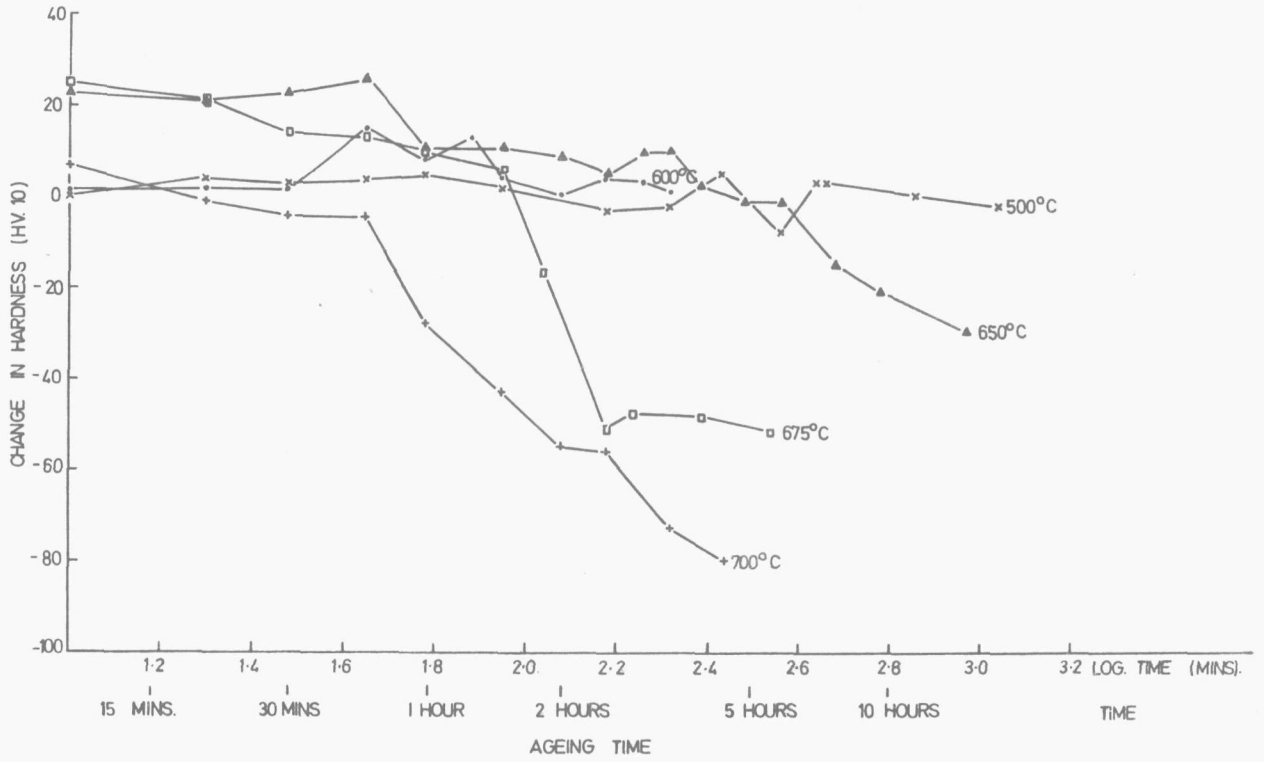

FIG. 29 SECONDARY HARDENING IN THE SIMULATED GRAIN COARSENED REGION OF DUCOL BW 87A (MATERIAL B)

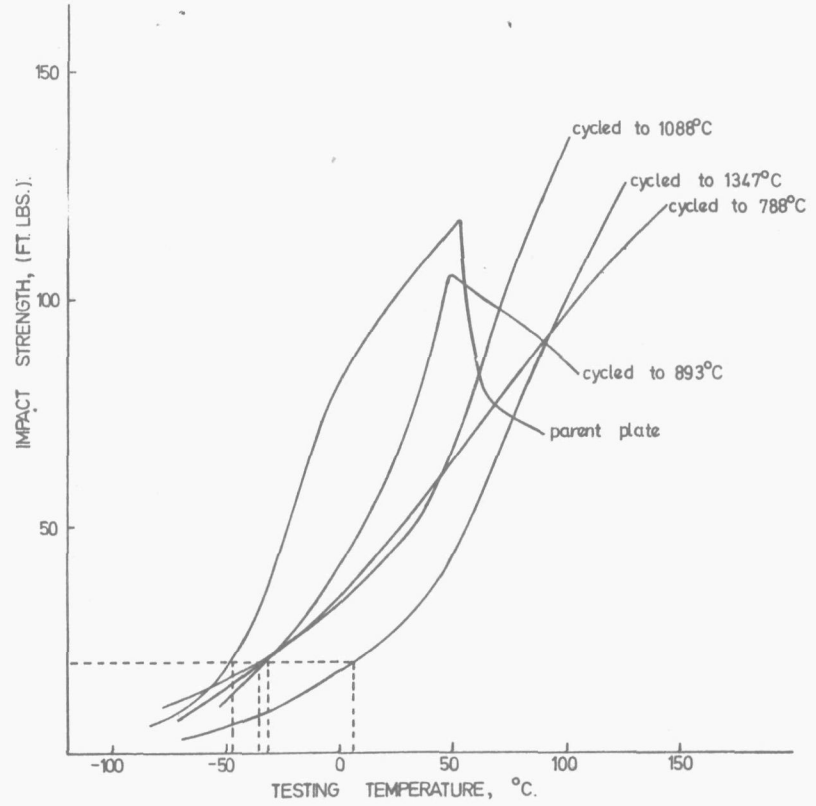

FIG. 30 COMPARISON OF CHARPY V-NOTCH IMPACT (FT. LBS) - TEMPERATURE FOR DUCOL W30 SIMULATED SPECIMENS (MATERIAL A)

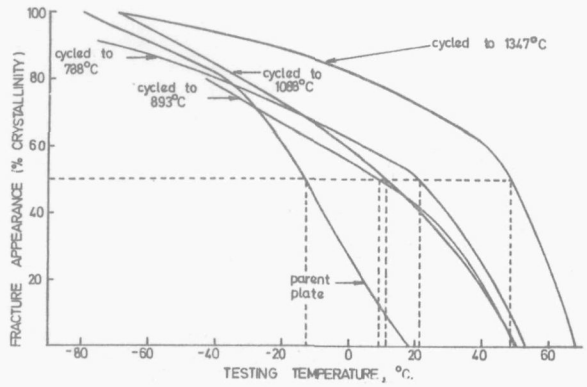

FIG. 31 COMPARISON OF CHARPY V-NOTCH IMPACT (% CRYSTALLINITY) - TEMPERATURE FOR DUCOL W30 SIMULATED SPECIMENS (MATERIAL A)

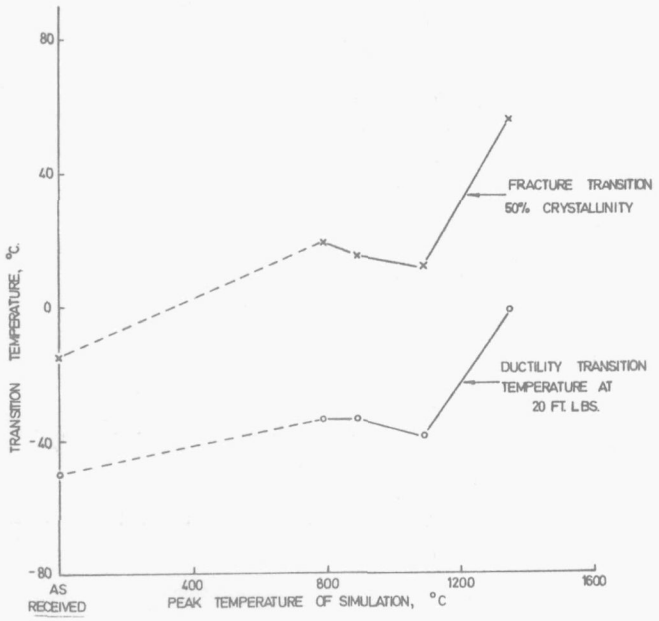

FIG. 32 VARIATION IN TRANSITION TEMPERATURE WITH PEAK TEMPERATURE OF SIMULATION FOR DUCOL W30 SPECIMENS (MATERIAL A)

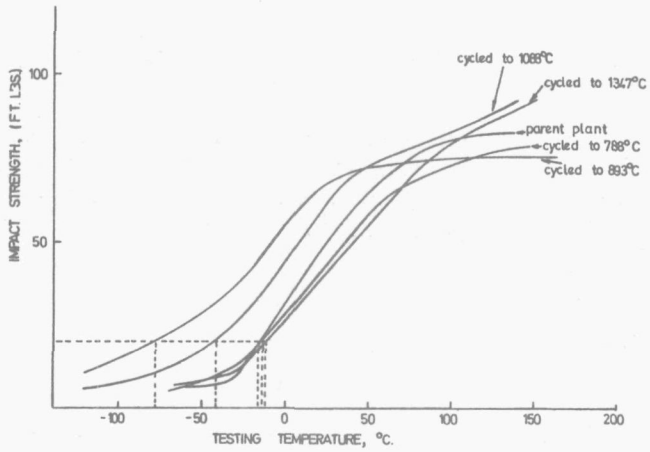

FIG. 33 COMPARISON OF CHARPY V-NOTCH IMPACT (FT. LBS) - TEMPERATURE FOR DUCOL BW87A SIMULATED SPECIMENS (MATERIAL B)

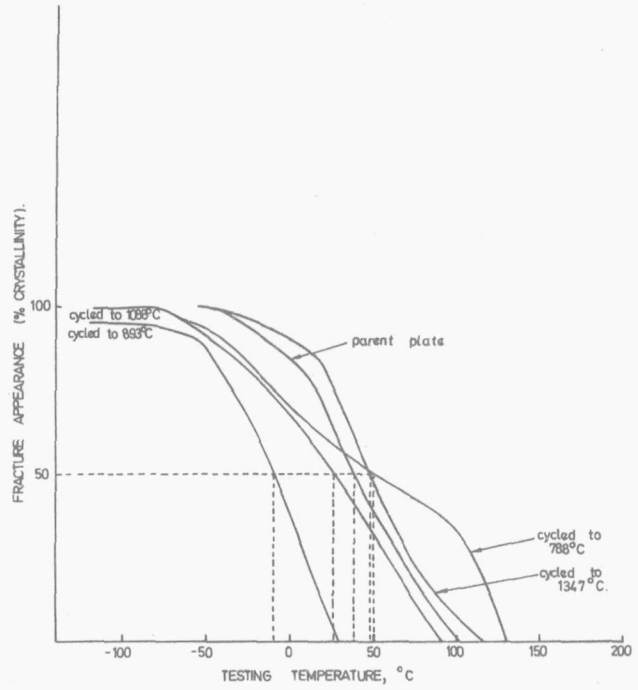

FIG. 34 COMPARISON OF CHARPY V-NOTCH IMPACT (% CRYSTALLINITY) - TEMPERATURE FOR DUCOL BW 87A SIMULATED SPECIMENS (MATERIAL B)

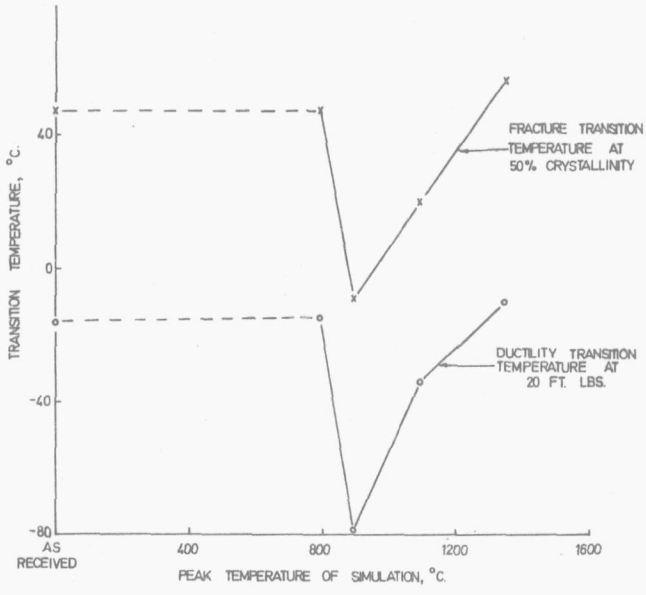

FIG. 35 VARIATION IN TRANSITION TEMPERATURE WITH PEAK TEMPERATURE OF SIMULATION FOR DUCOL BW 87A SPECIMENS (MATERIAL B)

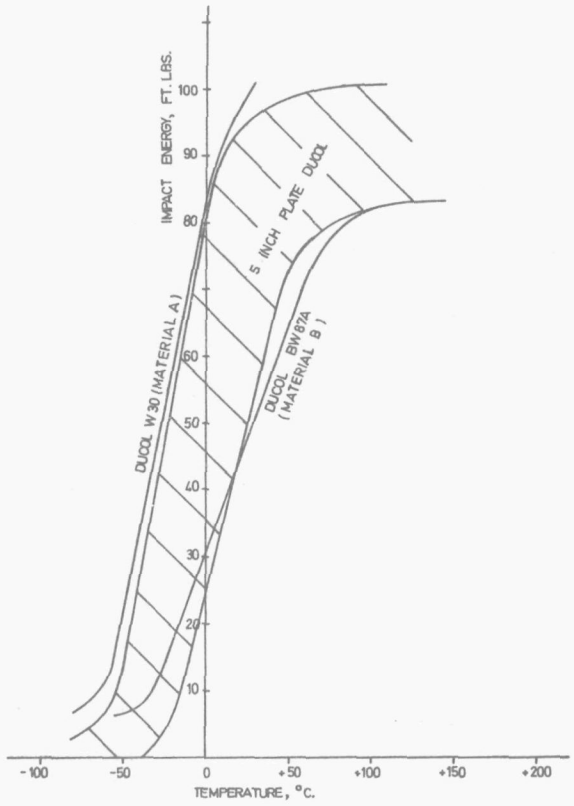

FIG. 36 CHARPY TRANSITION CURVES FOR PARENT MATERIALS